RAY, John Delbert, 1930-
NONLINEAR VIBRATIONS OF A CONTINUOUS
ELASTIC SYSTEM.

The University of Oklahoma, Ph.D., 1968
Engineering Mechanics

University Microfilms, Inc., Ann Arbor, Michigan

THE UNIVERSITY OF OKLAHOMA

GRADUATE COLLEGE

NONLINEAR VIBRATIONS OF A CONTINUOUS ELASTIC SYSTEM

A DISSERTATION

SUBMITTED TO THE GRADUATE FACULTY

in partial fulfillment of the requirements for the

degree of

DOCTOR OF PHILOSOPHY

BY

JOHN D. ELBERT RAY

Norman, Oklahoma

1968

NONLINEAR VIBRATIONS OF A CONTINUOUS ELASTIC SYSTEM

APPROVED BY

Charles W. Bert

William N. Huff

Franklin J. Appl

Davis M. Egle

Raymond Kaser

DISSERTATION COMMITTEE

ACKNOWLEDGMENT

The writer desires to express his sincere appreciation to his faculty advisor, Dr. Charles W. Bert, for the cooperation, encouragement, and assistance given during the preparation of this work.

The writer would also like to extend his thanks to Dr. William N. Huff, Dr. Frank Appl, Dr. Davis Egle, and Dr. Raymond Kaser for their valuable time and interest in editing this work.

This dissertation is dedicated to my wife, Doris, for her understanding, encouragement, and help.

TABLE OF CONTENTS

TABLE OF CONTENTS
(Continued)

LIST OF ILLUSTRATIONS

LIST OF ILLUSTRATIONS
(Continued)

NOMENCLATURE

a	=	half amplitude of vibration
A	=	cross-sectional area of beam
c	=	distance from neutral axis to outer fiber of beam
C,D	=	undefined constants
C_1	=	$EI/\rho A$
C_2	=	$N_o/\rho A$
C_3	=	$(EA/2\ell\rho A) \int_o^\ell v,_x^2 \, dx$
Cn	=	Jacobian elliptic cosine function
E	=	Young's modulus
f	=	frequency, cycles per second
F	=	force
h	=	beam thickness
I	=	area moment of inertia of cross section
J	=	mass moment of inertia
K	=	quarter period of Jacobian elliptic function
ℓ	=	length of beam
M	=	moment
n	=	positive integer
N	=	axial tensile force due to deflection
N_o	=	initial axial tensile force on beam

P_n = $n^2\pi^2 EI/\ell^2$ = Euler's load for a beam for buckling form with n half waves

Q = shear force

r = radius of gyration, $(I/A)^{1/2}$

R = a/h amplitude ratio

t = time

$T(t)$ = a function of time only

u = instantaneous longitudinal deflection of beam at any point x

v = instantaneous lateral deflection of beam at any point x

w = transverse load per unit length

$X(x)$ = a function of space x only

α = $n\pi/\ell$

α_1 = ℓ/π

γ = a/r

ε = strain

θ = angle of rotation

λ_1 = $(n\pi/\ell)^4$

λ_2 = $-(n\pi/\ell)^2$

ρ = beam mass per unit length

P = radius of beam curvature

σ_B = bending stress

σ_i = direct stress due to stretching load

σ_o = stress due to initial load

ϕ = variable of Jacobian elliptic function

ω = frequency, radians per second

NONLINEAR VIBRATIONS OF A CONTINUOUS ELASTIC SYSTEM

CHAPTER I

INTRODUCTION

Introductory Remarks

Nature is nonlinear; that is, mathematical models describing natural phenomena are often nonlinear functions. For some time nonlinear functions have been approximated by the introduction of linearizing assumptions into the solutions. Numerous papers have been published, many recently, in which linear superposition theory has been used for the solution of nonlinear partial differential equations. Ames [1][1] and Jones [2] explored using the superposition principle in the solution of nonlinear partial differential equations.

Rosenberg [3] defined the normal modes of a discrete-mass vibrating system in relation to the application of the superposition principle. Wah [4] summarized and extended these definitions to a nonlinear continuous system stating that a necessary but not sufficient condition for existence of normal modes is that the time and space variables must be separable. Wah went on to show that for large amplitude displacement of a beam with non-translating simple-

[1] Numbers in brackets indicate references at end of text.

supports, the normal modes are orthogonal, and the superposition principle should hold for the assumed space mode. (Hereafter this special beam system will be referred to as pin-ended.)

Wah further extended his work to the stability of normal modes of nonlinear continuous systems [5] by implying that for a pin-ended beam the time and space variables were separable and the normal modes could be defined, but that for non-simply supported continuous systems, the normal modes are not readily defined. Wah stated that this concept was difficult to accept.

Wah derived his concept from work that was done by Woinowsky-Krieger [6], in which the solution to the nonlinear equations of motion for the pin-ended beam were obtained by assuming a separation of time and space variables. The solution was derived by substituting an assumed sinusoidal space mode into the partial differential equation of motion and solving for the time function. Other investigators solved the basic equations of motion by other methods. McDonald [7] investigated a different approach in solving the basic equations of motion of a vibrating continuous system. Like Wah and others, McDonald directed his attention to the special case of pin-ended beam using the same equation of motion as obtained by Woinowsky-Krieger, etc. The solution to this equation was an assumed space mode in which the normal modes were coupled.

Other papers have been published describing the vibration of beams and plates in which a minimum energy or variational method [8-15] was used for the solutions.

Other investigators have obtained solutions based on the perturbation method [9, 10, 16]. Eringen [16] presented the solution for one and two term approximations. The solution with the one term approximation agreed closely with the results of Woinowsky-Krieger, and the second term approximation gave a solution that would require a vast amount of tedious computation.

Purpose

The purpose of this investigation is to study analytically and experimentally a particular continuous elastic system with emphasis on the large-deflection regime where the system is most nonlinear.

The system selected for this study is a pin-ended beam subjected to lateral vibrations. This system is selected because of its simplicity, and to emphasize a single nonlinearity.

Within the framework of the system there are two major possible nonlinearities that can be introduced into the equations of motion.

(1) One nonlinearity is caused by the pin ends not being allowed to move relative to the initial coordinates of the beam ends. This condition introduces a stretching strain in the beam as it is deflected from its initial position. The nonlinearity is introduced by the force due to stretching. The equation of motion is inherently nonlinear with the addition of this term, which is a function of position and time.

(2) The other major nonlinearity is caused by large beam deflection that invalidates the small-angle assumption which reduces the exact expression for the beam

curvature to the linear form. When the deflection becomes large, this assumption no longer holds, thus another nonlinearity is introduced into the equation of motion.

Fortunately, the nonlinearities mentioned above should not be emphasized to the same degree for a practical physical system. A system that has large enough deflection to produce the second nonlinearity will not have appreciable stretching since the ends will be allowed to move along the initial longitudinal axis of the beam. A beam with immovable ends may have appreciable stretching, but the deflection slope will have to be small for the system to be within elastic limits for most structural materials.

Both nonlinearities have been studied by many investigators. Woinowsky-Krieger [6], Wah [4, 5], Eringen [16], Burgreen [8], McDonald [7], and many others have studied the nonlinearity introduced into beams by the stretching and have assumed that the other nonlinearity can be neglected. Woodall [10], Warner [17], Wagner [18], Scott and Carver [19], and many others have studied the nonlinearity introduced by large deflections of the beam but de-emphasized the nonlinearity due to stretching of the beam.

Other investigators have extended the studies to nonlinearities of plates and shells. Wah [4], Somerset and Evan-Iwanowski [20], Eisley [21], Srinivasan [14, 15], Lurie [22], Mishenkov [23], and Wilson and Boresi [24] studied plates. The work of these investigators was analogous to that for beams and in some cases was directly applicable.

Wah [5], Burgreen [8], and Lurie [22] presented results of experimental investigations along with their analytical investigations.

In all cases, the maximum amplitude ratios (beam deflection/beam thickness) used were less than one half the maximum level obtained in this investigation.

The nonlinearity that is investigated here is the stretching introduced into the beam when the deflection is large, i.e., the ratio of deflection to beam thickness is above one, but does not exceed the elastic limit of the material.

Objectives

The objectives of this investigation are:

(a) to study the extent that the superposition and normal mode principles are applicable to the nonlinear equations of motion for a pin-ended beam.

(b) to present results obtained from experimental investigations on a vibrating beam of this type.

(c) to compare the experimental results with those predicted by theories obtained by other investigators.

CHAPTER II

ANALYSES

Introduction

As pointed out in the preceding chapter, for a pin-ended beam undergoing large-amplitude vibratory deflection, the nonlinearities are due to the stretching of the beam and the nonlinearity in the exact curvature expression. Within the framework of this investigation, only the stretching will be discussed and the nonlinearity in curvature will be neglected.

Equations of Motion

The equations of motion of an element of a pin-ended beam, as developed in Appendix A, are:

$$\rho A u_{,tt} = (N \cos\theta)_{,x} - (Q \sin\theta)_{,x} \quad (1)$$

$$\rho A v_{,tt} = (N \sin\theta)_{,x} + (Q \cos\theta)_{,x} - w \quad (2)$$

$$J\theta_{,tt} = -[Q \cos\theta + N \sin\theta]\ (1+u_{,x}) + [N \cos\theta - Q \sin\theta] + M_{,x} \quad (3)$$

where a subscript comma denotes partial differentiation with respect to the variables following the comma in the subscript.

These equations agree with the basic equations presented in Eringen's [16] and Woodall's [10] papers. There is an error in the equations presented by Eringen but it was corrected by Woodall.

The assumptions used to further develop the equations of motion from equations (1), (2), and (3) are:

(a) provision is made for a static tension,

(b) the beam material is homogeneous, isotropic, and obeys Hooke's Law,

(c) the cross section of the beam is uniform,

(d) a cross section of the beam, originally plane, remains plane and normal to the deformed axis,

(e) elastic deformation in the plane of the cross section is negligible,

(f) external and internal damping are neglected,

(g) the strain in the beam can be neglected when compared to unity, i.e.

$$(1 + u_{,x}) = 1, \tag{4}$$

(h) the angle of rotation of the section is small and the following approximations can be made:

$$\sin \theta \simeq \theta = v_{,x} \tag{5}$$

$$\cos \theta \simeq 1, \tag{6}$$

(i) since the thickness of the beam is small, rotatory inertia can be neglected, i.e.

$$J = 0, \tag{7}$$

(j) there is no external load applied directly to the beam, i.e.

$$w = 0. \tag{8}$$

Applying these assumptions, equations (1), (2), and (3) become:

$$N_{,x} - (Q\theta)_{,x} = 0 \tag{9}$$

$$(N\theta)_{,x} + Q_{,x} = \rho A v_{,tt}, \tag{10}$$

and

$$M_{,x} - (Q + N\theta) + (N - Q\theta) = 0. \tag{11}$$

After integration with respect to x, equation (9) becomes:

$$N - Q\,\theta = C, \tag{12}$$

where C is a constant of integration.

The beam is initially straight, when $\theta_o = 0$, and the only load applied to the system is the initial axial load on the beam; therefore,

$$N_o = C, \tag{13}$$

and equation (12) becomes,

$$N - Q\theta = N_o \tag{14}$$

or

$$N = N_o + Q\theta. \tag{15}$$

Substituting equation (15) into equation (11), one obtains the following results:

$$M_{,x} = Q(1 + \theta^2) - N_o(1 - \theta) \tag{16}$$

$$M_{,xx} = Q_{,x}\,(1 + \theta^2) + 2Q\theta\theta_{,x} + N_o\theta_{,x}. \tag{17}$$

It is shown in Appendix A that when stretching is introduced, the relationship between moment, M, and deflection, v, becomes:

$$M = EIv_{,xx}/(1 + \theta^2)^{3/2} - N(EI/EAc). \tag{18}$$

Using the assumption that θ^2 can be neglected when compared to unity and the coordinate system established in Appendix A, equation (18) becomes:

$$M = -EI\ (v_{,xx} - N/EAc), \tag{19}$$

equation (16) becomes:

$$Q = \{-[EI\ V_{,xxx} - N_{,x}/EAc)] - N_o\ (1 - \theta)\}/(1 + \theta^2), \tag{20}$$

and equation (20) becomes, after differentiating with respect to x and neglecting θ^2:

$$Q_x = -\ EI\ (v_{,xxxx} - N_{,xx}/EAc) - 2Q\theta\theta_{,x} + N_o\ \theta_{,x}. \tag{21}$$

Substituting equation (21) into equation (10), after equation (10) is expanded, the results yield:

$$\begin{aligned} \rho A v_{,tt} = N_{,x}\theta + N\theta_{,x} + N_o\theta_{,x} - EI(v_{,xxxx} - N_{,xx}/EAc) \\ - 2Q\theta\theta_{,x}, \end{aligned} \tag{22}$$

$$\begin{aligned} \rho A v_{,tt} = N_{,x}\theta\ [1 - 2\ (EI/EAc)\ \theta_{,x}] + (EI/EAc)\ N_{,xx} \\ + N\theta_{,x} + N_o\theta_{,x} - EI(v_{,xxxx} - 2v_{,xxx}\theta\theta_{,x}). \end{aligned} \tag{23}$$

In Appendix A, the following expressions for the average internal tension, N, and the changes in internal tension are developed as:

$$N = (EA/2)\ \int_{x_o}^{x_1} v_{,x}^{\ 2}\ dx / \int_{x_o}^{x_1} dx, \tag{4C}$$

$$N_{,x} = (EA/2)\ v_{,x}^{\ 2}\ , \tag{3C}$$

and

$$N_{,xx} = EA\ v_{,x}\ v_{,xx}\ . \tag{5C}$$

It can be seen that when $N_{,x}$ is introduced into equation (23), the first term becomes a θ^3 term which can be neglected.

If the internal tension force, N, is introduced into equation (23) as an average force across the entire length of the beam,

$$N = (EA/2\ell)\int_0^\ell v_{,x}^{2}\ dx \tag{25}$$

then equation (23) becomes:

$$\rho A v_{,tt} = [N_o + (EA/2\ell)\int_0^\ell v_{,x}^{2}\,dx]\,\theta_{,x} - EI\,v_{,xxxx}$$

$$+ EI\,(c^{-1} + 2v_{,xxx})\,\theta\theta_{,x}. \tag{26}$$

Equation (26) agrees with the equation of motion derived by Wah, Woinowsky-Krieger, etc. except for the last term.

It will be shown later, in the development of the Ritz-Galerkin method of solution, that the last term can be neglected for the class of beams used in this investigation.

When this term is dropped, equation (26) becomes:

$$\rho A v_{,tt} = -\,EI\,v_{,xxxx} + [N_o + (EA/2\ell)\int_0^\ell v^2_{,x}\,dx]\,v_{,xx}. \tag{27}$$

<u>Solution of Equation of Motion</u>

Assumed Space Mode

Equation (27) is in the form of a nonlinear partial differential equation, where the nonlinear terms are introduced by the stretching force. The displacement function, v, is differentiated with respect to time, t, and space variable, x, but nowhere in the equation is v differentiated with respect to x and t together. This indicates that there should be an expression for displacement in which time and space are separated variables.

Introducing the displacement function as separated-variables in the form:

$$v = X(x)\ T(t), \tag{28}$$

equation (27) becomes:

$$T_{,tt} = [-(EI/\rho A)X_{,xxxx}/X + (N_o/\rho A)X_{,xx}/X]\ T$$
$$+ \{[(EA/2\ell\rho A)/ \int_o^\ell X^2_{,x}\ dx]\ X_{,xx}/X\}\ T^3. \tag{29}$$

Because of the T^3 term the variables will not separate neatly as they do in linear differential equations.

Assuming the space mode function of equation (28) to be of a simple form:

$$X = a \sin \alpha x. \tag{30}$$

The boundary conditions for a pin-ended beam are

$$X = X_{,xx} = 0 \text{ at } x = 0,\ \ell. \tag{31}$$

The function will satisfy the boundary conditions when either a is zero, which is the trivial solution, or when

$$\sin \alpha x = 0, \tag{32}$$

which occurs when

$$\alpha = n\pi/\ell \quad ; \quad n = 0,\ 1,\ 2,\ 3\ ---\ . \tag{33}$$

When the boundary condition for the shear force is introduced into the modal function, the additional restrictions are placed on the solution. When no external force is applied to the system except for the inertial force, then the shear forces at each end of the beam are equal in magnitude. If the shear forces are the same sign, then

$$v_{,xxx}\Big|_{x=0} = v_{,xxx}\Big|_{x=\ell}\ ; \tag{34}$$

which implies that

$$\cos n\pi = 1;$$

this occurs when n is even, or

$$n = 0,\ 2,\ 4\ ---\ 6.$$

If the shear forces are opposite in sign, then

$$v_{,xxx}\Big|_{x=0} = -v_{,xxx}\Big|_{x=\ell}, \tag{35}$$

which implies that

$$\cos n\pi = -1, \tag{36}$$

this occurs when n is odd, or

$$n = 1, 3, 5 --- .$$

The condition for the shear forces to be of the same sign is when the displacement function is asymmetric about the center of the beam length. The condition for the shear forces to be opposite sign is when the displacement function is symmetric. The case of base excitation is a symmetric displacement and only the odd harmonics are excited.

Applying equation (30) to equation (29), the results yield:

$$T_{,tt} = [-C_1\ (n\pi/\ell)^4 + C_2\ (n\pi/\ell)^2]T + C_3\ (n\pi/\ell)^2\ T^3, \tag{37}$$

where $C_1 = EI/\rho A$ (38)

$$C_2 = N_o/\rho A \tag{39}$$

$$C_3 = (EA/2\ell\rho A) \int_o^\ell v_{,x}{}^2\ dx. \tag{40}$$

As shown by Woinowsky-Krieger, equation (37) suggests a solution in the form of a Jacobian elliptic cosine function,

$$T = Cn\ (pt,\ k), \tag{41}$$

where Cn = Jacobian elliptic cosine function,

$$p^2 = (n\pi/\ell)^4\ (EI/\rho A)\ (1 + \gamma^2/4) + (n^2\pi^2/\ell^2)(N_o/\rho A), \tag{42}$$

and $k^2 = \{2 + 8/\gamma^2[1 + (N_o\ell^2/n\pi^2\ \ EI)]\}^{-1}.$ (43)

When the quantities for $X(x)$ and $T(t)$ are substituted into equation (28), the results yield:

$$v = a\ \sin\ (n\pi x/\ell)\ Cn\ (pt,\ k). \tag{44}$$

The resonant frequency of the system will be the inverse of the period of the Jacobian elliptic cosine function. The period of the function Cn (pt, k) is:

$$4K = 4 \int_{0}^{\pi/2} (1 - k^2 \sin^2 \Phi)^{-1/2} \, d\Phi \tag{45}$$

and the corresponding frequency is:

$$\omega = (\pi p/2K). \tag{46}$$

Assumed Time Mode

Another approach to the solution to the equation of motion, (27), is to assume a time mode for equation (28) and to solve for the space mode.

Assuming the time mode to be of a simple form:

$$T = \sin \omega t, \tag{47}$$

then equation (29) becomes

$$-\omega^2 \sin \omega t = [-C_1 (X_{,xxxx}/X) + C_2 (X_{,xx}/X)] \sin \omega t + C_3 (X_{,xx}/X) \sin^3 \omega t. \tag{48}$$

There are two methods for expanding equation (48) to simplify the equation into a closed form solution. Each of these methods involves the expansion of the $\sin^3 \omega t$ term. They differ in the form of the expression and in the higher-harmonic terms neglected.

In the first approach, the $\sin^3 \omega t$ term is expanded by using the trigonometric identity:

$$\sin^3 \omega t = (3/4) \sin \omega t - (1/4) \sin 3 \omega t.$$

Then, after collecting terms, equation (48) becomes:

$$\{C_1 X_{,xxxx} - [C_2 + (3/4) C_3] X_{,xx} - (\omega^2) X\} \sin \omega t + (1/4) C_3 \sin 3\omega t = 0. \tag{49}$$

The solution to equation (49) would contain third harmonic terms. Since only the fundamental frequency is of interest, the sin $3\omega t$ term is neglected. Equating the bracketed term of sin ωt to zero gives:

$$C_1 X_{,xxxx} - [C_2 + (3/4)\ C_3]\ X_{,xx} - \omega^2 X = 0. \quad (50)$$

Assuming a solution of an exponential form

$$X = e^{\beta x}, \text{ and}$$

substituting into equation (49),

$$\beta = \pm 1/2\ C_1^{-1} \{(C_2 + 3C_3/4) \pm [(C_2 + 3C_3/4)^2 + 4C_1\omega^2)]^{1/2}\}^{1/2},$$

then

$$\beta = \pm 1/2\ C_1^{-1} \{C_2 + 3C_3/4 + [(C_2 + 3C_3/4)^2 + 4C_1\omega^2]^{1/2}\}^{1/2}, \quad (51)$$

and

$$\beta = \pm 1/2\ C_1^{-1} \{[(C_2 + 3C_3/4)^2 + 4C_1\omega^2]^{1/2} - (C_2 + 3C_3/4)\}^{1/2} \quad (52)$$

or $\beta = \beta_1,\ -\beta_1,\ i\beta_2,\ -i\beta_2.$

These give a solution of the form:

$$X = A_1 \sin \beta_2 x + A_2 \cos \beta_2 x + A_3 \sinh \beta_1 x + A_4 \cosh \beta_1 x \quad (53)$$

The boundary conditions are again:

$$X = X_{,xx} = 0 \quad \text{at} \quad x = 0,\ \ell,$$

which implies that

$$A_2 = A_3 = A_4 = 0,$$

and that

$$A_1 = a \text{ and } \beta_2 = n\pi/\ell.$$

Using equation (52),

$$\omega^2 = \{[(n\pi/\ell)^4\ C_1 + (n\pi/\ell)^2\ (C_2 + 3C_3/4)]\}. \quad (54)$$

After substituting equations (33), (34), and (35) into equation (54) and evaluating the integral, one obtains:

$$\omega^2 = (n\pi/\ell)^4 \, (EI/\rho A)[1 + (3/16)\gamma^2] + (n\pi/\ell)^2 \, (N_o/\rho A). \qquad (55)$$

Since the resonant frequency of a linear pin-ended beam is defined as:

$$\omega_o^2 = (n\pi/\ell)^4 (EI/\rho A) \qquad (56)$$

and the buckling load of the beam buckling as an Euler column is defined as:

$$P_n = (n\pi/\ell)^2 \, EI, \qquad (57)$$

then equation (55) becomes:

$$\omega^2 = \omega_o^2 \, [1 + (3/16)\gamma^2 + (N_o/P_n)] \qquad (58)$$

and

$$X = a \sin (n\pi x/\ell).$$

The second approach in the solution of equation (48) is by arranging the equation into the following form:

$$[C_1 \, X_{,xxxx}/X - (C_2 + C_3 \sin^2 \omega t)(X_{,xx}/X) - \omega^2] \sin \omega t = 0. \qquad (59)$$

Expanding

$$\sin^2 \omega t = (1/2)(1 - \cos 2\omega t)$$

and substituting into equation (59), the results yield:

$$[C_1 \, X_{,xxxx} - (C_2 + C_3/2) \, X_{,xx} - \omega^2 X] \sin \omega t$$
$$+ (C_3/2) \cos 2\omega t = 0 \qquad (60)$$

The cos $2\omega t$ term is neglected since, as before, it implies there are second harmonic terms in the solutions.

Equating the bracketed term of the sin ωt to zero and solving the equation, as was done previously, the solutions for X and the resonant frequencies become:

$$X = a \sin n\pi x/\ell,$$

$$\omega^2 = \omega_o^2 \, [1 + (\gamma^2/8) + (N_o/P_n)]. \tag{61}$$

As noted when comparing equations (58) and (61), the only change is due to the constant of γ^2 term.

In both of the approaches when the assumed time mode for solution is used, the displacement takes the form

$$v = a \sin (n\pi x/\ell) \sin \omega t. \tag{62}$$

Ritz-Galerkin Approach

Srinivasan [14, 15] used the Ritz-Galerkin approach to obtain a solution to equation (27). In his work he followed the approach of Arnold [25] for dynamic systems, except Srinivasan used one-term-approximations of the form:

$$v(x,t) = C \sin \alpha x \quad \sin \omega t \tag{63}$$

where $\alpha = n\pi/\ell$, and C is the unknown parameter.

One form of the Ritz-Galerkin procedure requires that

$$\int_0^{2\pi/\omega} \int_0^{\ell} \overline{DE} \; \Phi \; dx \; dt = 0, \tag{64}$$

where $\overline{DE}$ is the differential equation (29) with equation (63) substituted for $v(x,t)$, and Φ is the assumed function. Applying the values to equation (64), one obtains:

$$\int^{2\pi/\omega} \int_0^{\ell} C \, \{ \omega^2 \sin \alpha x \sin \omega t + C_1 \, \alpha^4 \, (\sin \alpha x \sin \omega t)$$

$$+ C_2 \, \alpha^2 \sin \alpha x \sin \omega t$$

$$+ [EAC^2/2\ell \int_0^{\ell} (\cos^2 \alpha x) \, dx] \sin^3 \omega t \sin \alpha x\}$$

$$\sin \alpha x \sin \omega t \; dx \; dt = 0. \tag{65}$$

The integrals appearing in equation (65) are evaluated as follows:

$$\int_0^{2\pi/\omega} \int_0^{\ell} \omega^2 \sin^2 \alpha x \sin^2 \omega t \, dx \, dt = \omega^2 (\ell/2)(\pi),$$

$$\int_0^{2\pi/\omega} \int_0^{\ell} C_1 \alpha^4 \sin^2 \alpha x \sin^2 \omega t \, dx \, dt = C_1 \alpha^4 (\ell/2) (\pi),$$

$$\int_0^{2\pi/\omega} \int_0^{\ell} C_2 \alpha^2 \sin^2 \alpha x \sin^2 \omega t \, dx \, dt = C_2 \alpha^2 (\ell/2) (\pi),$$

$$\int_0^{2\pi/\omega} \int_0^{\ell} (EAC^2/2\ell)\left[\int_0^{\ell} (\cos^2 \alpha x) \, dx\right] \sin^2 \alpha x \sin^4 \omega t \, dx \, dt$$

$$= EAC^2/4 (\ell/2) (3\pi/4).$$

Therefore equation (65) becomes:

$$[-\omega^2 + C_1 \alpha^4 + C_2 \alpha^2 + EAC_1 (3/16 C^2)](\pi\ell/2) = 0. \qquad (66)$$

Constant C is equal to the amplitude of displacement of the beam, and equation (66) reduces, after solving for the resonant frequencies, to:

$$\omega^2 = \omega_o^2 (1 + 3/16 \gamma^2 + N_o/P_n).$$

This is the same equation as obtained from the first approach of the assumed-time-mode technique, and is analogous to the equation obtained by Srinivasan [14, 15].

Using a two-term space-modal approximation for the solution, when applying the Ritz-Galerkin technique, the assumed function is:

$$v (x,t) = \sin \omega t (C \sin \alpha_1 x \pm D \sin 3\alpha_1 x),$$

where $\alpha_1 = \pi/\ell$.

The solutions for the resonant frequencies are:

$$\omega^2 = \omega_o^2 \,[1 + 3/16\ (\gamma_1^2 \pm \gamma_3^2) + N_o/P_n] \tag{67}$$

and

$$\omega^2 = 9\omega_o^2 \,[1 + 3/16\ (\gamma_1^2 \pm \gamma_2^2) + N_o/P_n]. \tag{68}$$

where $\gamma_1^2 = C^2/r^2$ and $\gamma_2^2 = D^2/r^2$, r^2 = I/A radius of gyration.

Equation (68) differs from equation (67) by only a constant multiplier. Thus, these equations are dependent equations and the assumed constants (C and D) cannot be determined.

This expression is analogous to that obtained by Srinivasan [15], except that he had an external-loading term which removed the dependency mentioned above and permitted him to obtain numerical values for C and D as a function of the force amplitude.

However, his plots indicated that the coupling effects are small compared to the fundamental mode but increase to a peak of approximately 10 percent of the fundamental amplitude.

With the assumed displacement function as:

$$v\ (x,t) = a \sin \alpha x\ (D_1 \sin \omega t + D_2 \sin 3\omega t),$$

the solutions of the resonant frequencies are:

$$\omega^2 = \omega_o^2\ [1 + (3/16r^2)(D_1^2/2 - D_1 D_2 + 2D_2^2) + N_o/P_n] \tag{69}$$

and

$$\omega^2 = (1/9)\ \omega_o^2\ \{1 + (3/16r^2)[-2D_1^3/(3D_2) + 2D_1 D_2 + D_2^2] + N_o/P_n\} \tag{70}$$

Returning to equation (26):

$$\rho AV_{,tt} = [N_o + (EA/2\ell) \int_o^\ell v_{,x}^2 \, dx] \; v_{,xx} - EI \; v_{,xxxx}$$

$$+ EI \; (1/c + 2v_{,xxx}) \; v_{,x} \; v_{,xx}]. \tag{26}$$

Solving the equation by a Ritz-Galerkin technique with a one-term approximation of the form,

$v(x\ t) = a \sin \alpha x \sin \omega t$, equation (26) becomes:

$$\int_o^{2\pi/\omega} \int_o^\ell a \; \{\omega^2 \sin \alpha x \sin \omega t + C_1 \; \alpha^4 \; (\sin \alpha x \sin \omega t)$$

$$+ C_2 \; \alpha^2 \sin \alpha x \sin \omega t + [EAa^2/2\ell \int_o^\ell \cos^2 \alpha x \, dx]$$

$$\alpha^4 \sin^3 \omega t \sin \alpha x + C_1 \; (a^2/c + 2\alpha^3 \; a^3 \cos \alpha x \sin \omega t)$$

$$(\alpha^3 \sin \alpha x \cos \alpha x \sin^2 \omega t)\} \sin \alpha x \sin \omega t \, dx \, dt = 0 \tag{71}$$

All the integrals of equation (71) are the same as presented before except for the last term in which

$$\int_o^{2\pi/\omega} \int_o^\ell (\sin^2 \alpha x \cos \alpha x) \sin^3 \omega t \, dx \, dt$$

$$= (1/3)\alpha \sin^3 \alpha x \Big|_o^\ell = 0$$

and $$\int_o^{2\pi/\omega} \int_o^\ell (\sin^2 \alpha x \cos^2 \alpha x \sin^4 \omega t) \, dx \, dt = 3\pi\ell/32\omega.$$

When these integrals are applied to equation (26), the equation for the resonant frequencies become:

$$\omega^2 = \omega_o^2 \; [1 + (3/16)\gamma^2 + N_o/P_n + (3/16)(n\pi a/\ell)^2]. \tag{72}$$

When the beam modal deflection, na, is small in comparison to the length, ℓ ($na/\ell \approx 0$), then the last term of equation (72) can be neglected. The modal numbers for a pin-ended beam will have to be small in comparison to the length for the material to remain within its elastic limits.

Reviewing: There are three basic solutions to the equation of motion, each using a different approach.

(1) assumed space mode:

$$\omega^2 = p/4K$$

$$v(x,t) = a \sin n\pi x/\ell \; \mathrm{cn}\,(pt,k),$$

(2) assumed time mode:

(a) $\omega^2 = \omega_o^2\,[1 + (3/16)\gamma^2 + N_o/P_n]$

$$v(x,t) = a \sin (n\pi x/\ell) \sin \omega t$$

(b) $\omega^2 = \omega_o^2\,[1 + (\gamma^2/8) + N_o/P_n]$

$$v(x,t) = a \sin (n\pi x/\ell) \sin \omega t$$

(3) Ritz-Galerkin method:

$$\omega^2 = \omega_o^2\,[1 + (3/16),, \quad + N_o/P_n]$$

$$v(x,t) = a \sin (n\pi x/\ell) \sin \omega t.$$

Stress

The stress applied to the beam is a combination of all the stress components included in the basic equation of motion.

(a) Bending:

Using the assumption that plane sections remain plane under deflection, the bending stress can be determined from

$$\sigma_B = Mc/I. \tag{73}$$

(b) Initial tension load:

It is not possible to suspend a beam in the horizontal plane without the beam being deflected initially. An external load is necessary to extend the beam to an initially straight position. The initial tensile stress will be:

$$\sigma_o = N_o/A. \tag{74}$$

(c) Stretching tension load:

This stress can be determined from the expression for stretching load:

$$N = (EA/2\ell) \int_o^\ell v,_x^2 \, dx, \tag{25}$$

substituting the expression derived for deflection:

$$v(x,t) = a \sin (n\pi x/\ell) \sin \omega t,$$

the stress function becomes:

$$\sigma_i = (n\pi/\ell)^2 (EI/4A)\gamma^2 \sin^2 \omega t. \tag{75}$$

It can be seen that the stress function will attain a maximum value of

$$\sigma_i = (n\pi/\ell)^2 (EI/4A)(\gamma^2) \tag{76}$$

twice during each cycle. Introducing the Euler buckling load, P_n, the stress expression becomes:

$$\sigma_i = (P_n/4A)\gamma^2. \tag{77}$$

In the cases investigated experimentally, the data are presented as a function of the beam thickness.

Introducing the quantity

$$R = a/h;$$

then $\gamma^2 = 12R^2$ for a rectangular beam. (78)

Applying R to equations (42) and (43), the results yield:

$$p^2 = \omega_o^2 \; (1 + 3R^2 + N_o/P_n) \tag{79}$$

$$k^2 = [2 + (2/3)R^{-2} \; (1 + N_o/P_n)]^{-1}, \tag{80}$$

equation (58) becomes:

$$\omega^2 = \omega_o^2(1 + 2.25R^2 + N_o/P_n), \tag{81}$$

equation (61) becomes:

$$\omega^2 = \omega_o^2 \; (1 + 1.5R^2 + N_o/P_n), \tag{82}$$

equation (66) becomes:

$$\omega^2 = \omega_o \; (1 + 2.25R^2 + N_o/P_n) \tag{83}$$

and equation (77) becomes:

$$\sigma_i = 3R^2 \; P_n/A. \tag{84}$$

CHAPTER III

EXPERIMENTAL INVESTIGATION

Introduction

Forced-vibration experiments were conducted on a beam, simply-supported between fixed supports, to investigate limitations on theoretical analyses. The effects that were investigated were:

(a) resonant frequency as a function of deflection and initial tension,

(b) tension stress as a function of deflection and position,

(c) modal shape as a function of deflection.

Specimen

The specimen selected for this investigation was a beam 0.50 inches wide, 0.032 inches thick, and 20.0 inches long measured from the centers of the pins. The material of the beam was Ti-75A, DMS 1536D, titanium alloy. This material was selected because of its moderate modulus of elasticity, low density, and high strength.

Shown on Figure 1 is a typical stress-strain curve for Ti-75A titanium alloy. One of the curves that is shown was taken from a military handbook [26], and the other curve was taken from stress-strain experimental data that were obtained on some samples of the material.

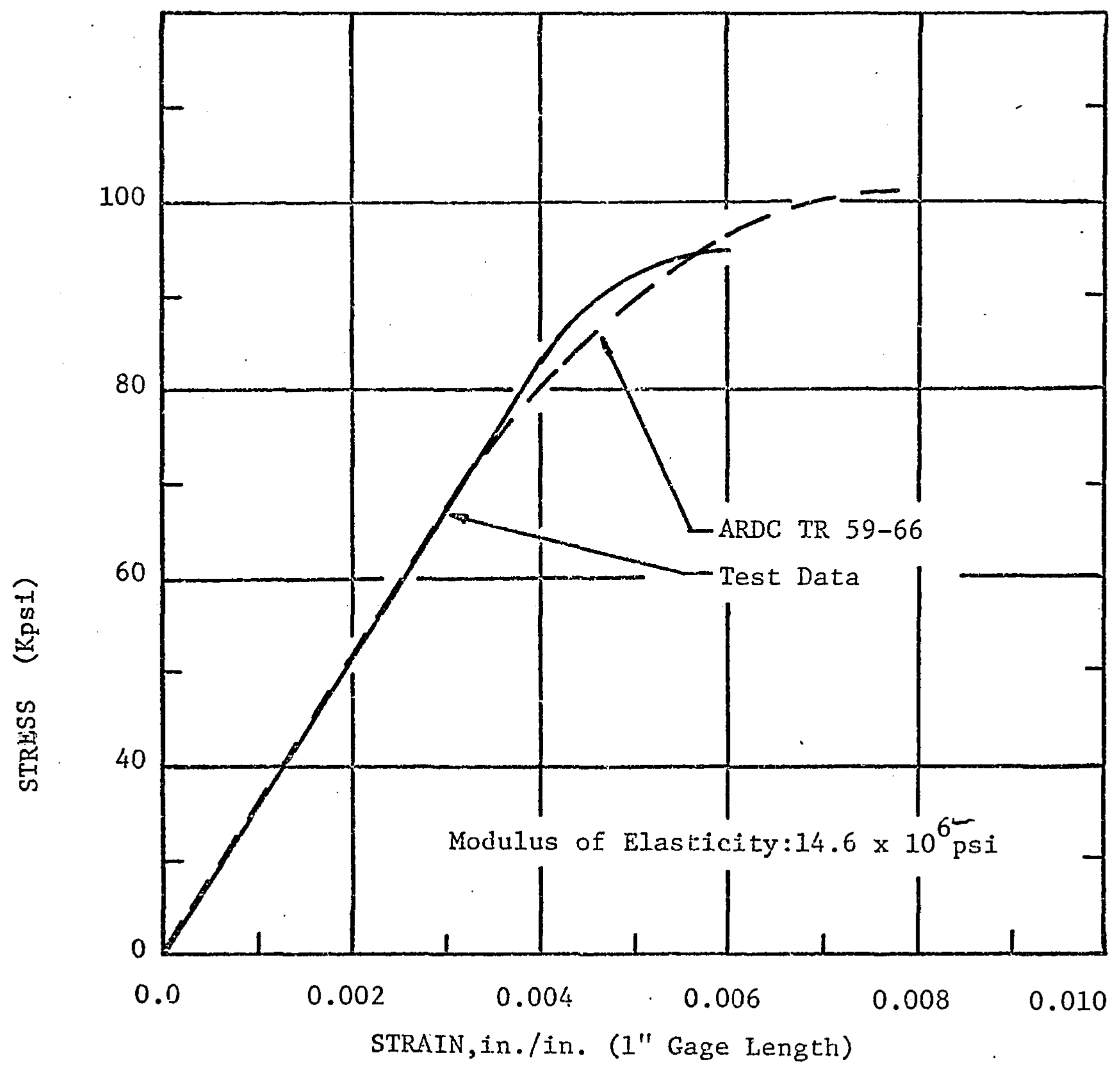

TITANIUM EXPERIMENTAL STRESS-STRAIN CURVES

FIGURE 1

The measured data values for the material were:

Modulus of Elasticity	14.6×10^6 psi
Specific Weight	0.186 pounds/cu. in.
Tensile Yield Strength (0.2% offset)	70 kpsi
Tensile Ultimate Strength	90 kpsi

The dimensions of the beam were selected so that the basic assumptions in the theoretical analyses would be valid. The length of the specimen was selected to give a large length to thickness ratio so that shear deformation could be neglected. The thickness of the beam was selected to give large deflections without exceeding the elastic limit of the material. The width of the beam was reduced to a minimum so that "plate effects" could be neglected. The 0.50-inch width was judged to be the minimum width on which an electric-resistance strain gage could be applied. The small cross-sectional area of the beam allowed rotatory inertia to be neglected.

Test Fixture

The specimen was suspended between two pins, free to rotate but restrained from translation. Figure 2 shows schematically the beam suspended in the test rig and the test-rig dimensions. Figure 3 is a photograph of the test rig and the suspended specimen. The base of the fixture was made of 3/4-inch aluminum plate that adapted the test fixture to the head of the electrodynamic exciter (M-B Mfg., Model C-10, 1250 pounds maximum-force capacity). Attached to the adapter plate was a 4-inch aluminum I beam. On each end of the I beam's top was an aluminum pillar block. The pillar blocks contained the attachments for the pin ends. The attachments were slotted shafts that were fixed

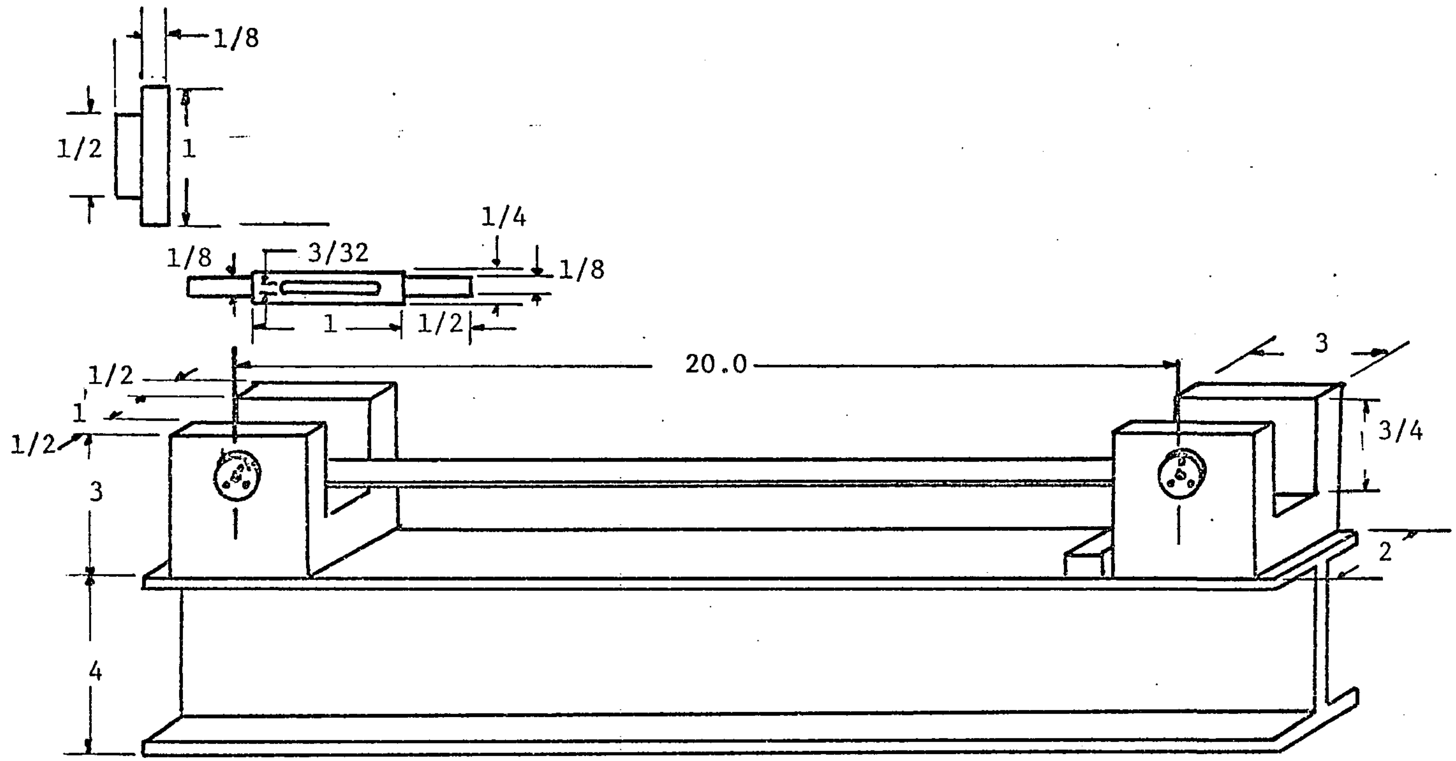

ALL DIMENSIONS IN INCHES

SCHEMATIC OF TEST RIG WITH SPECIMEN

FIGURE 2

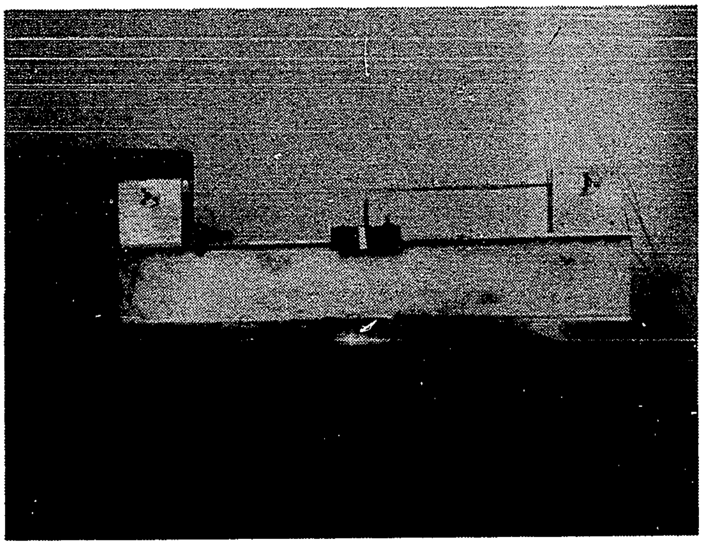

PHOTOGRAPH OF TEST RIG WITH SPECIMEN

FIGURE 3

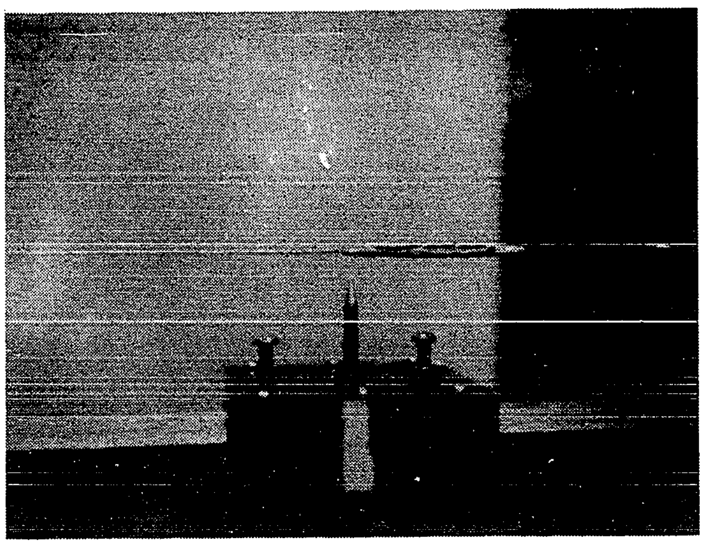

PHOTOGRAPH OF GAGING MECHANISM

FIGURE 4

to pillar blocks by two sets of roller bearings (Fafnir Model B-33KDD5). The specimen was held into the slot in the shaft by three #4-40 screws. One of the pillar blocks was fixed permanently to the I beam, and the other was made adjustable along the length of the I beam. An adjustment block was fixed to the I beam; the block contained two screws that pushed against each side of the pillar block's face. This set-up was used to adjust the initial tension load on the specimen and to remove the clearance in the roller bearings. Once the initial load was set on the specimen, the pillar block was attached rigidly to the I beam.

The deflection of the specimen was gaged by the sliding block in the middle of the I beam. A pointed screw with locking nut was inserted into the block. The method that was used to measure the beam deflection will be discussed in the test procedure section. Figure 4 shows a close-up photograph of the gaging mechanism.

Instrumentation

Dynamic strain gages were attached to the specimen at various locations. Three different strain-gage-location patterns were used. All of these patterns are shown in Figure 5.

For the first pattern, the strain gages were located at most of the vibration antinodes for the first, third, fifth and seventh resonant modes.

For the second pattern, two strain gages were located at the center, top and bottom, of the specimen which was at the vibration antinode for all the odd modes. For this test pattern an electronic stroboscope (General Radio Strobotac, type 1531-AB) was introduced into the test equipment; therefore, it was not necessary to have the

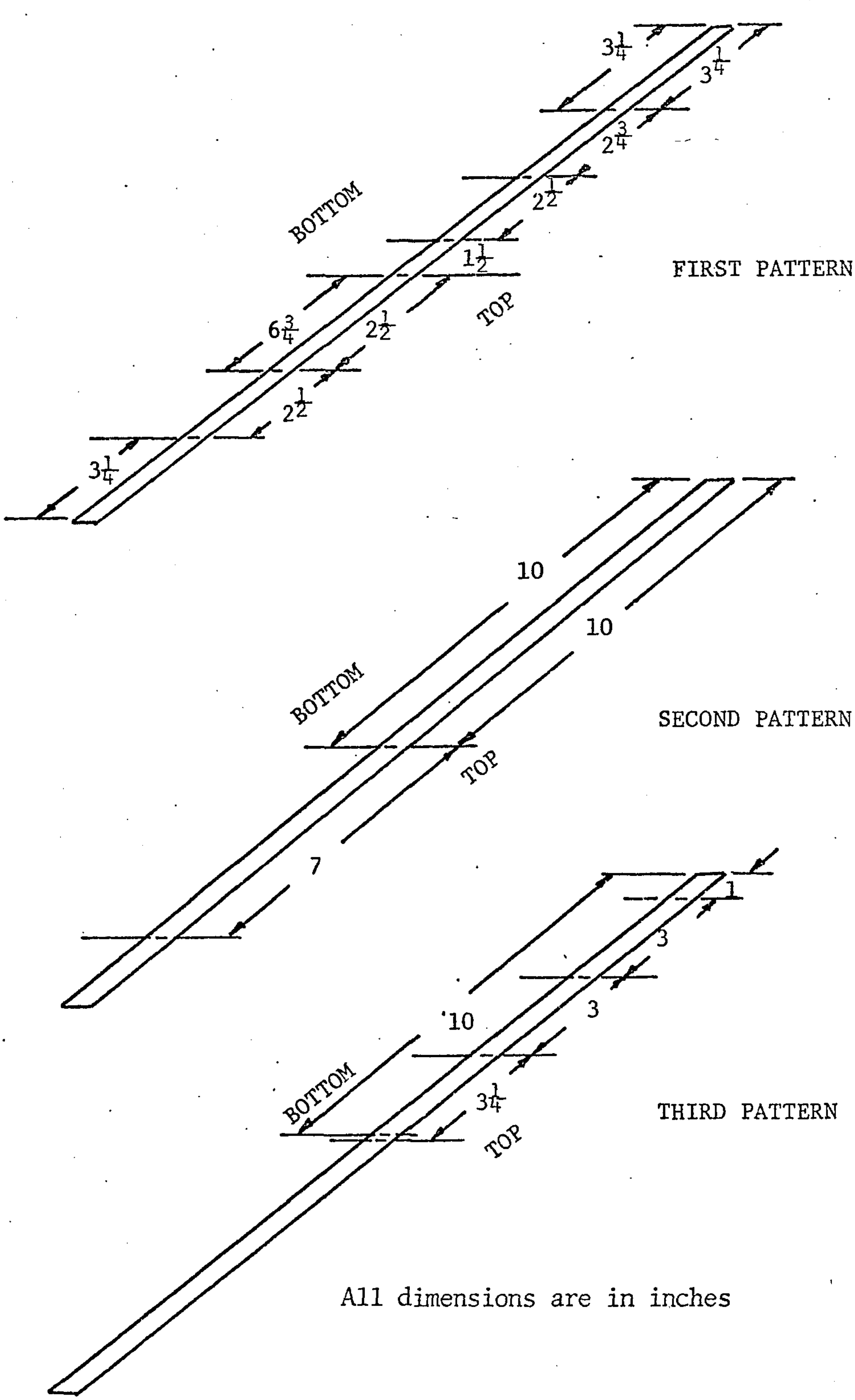

STRAIN-GAGE LOCATIONS

FIGURE 5

extra strain gages to investigate the modal shapes. The stroboscope, in conjunction with a camera (Polaroid Model 250), was used to capture the modal shapes. A third gage was located near one of the pin ends so that the initial tension could be monitored throughout the test.

For the third pattern, the strain gages were located at equal intervals along the specimen, from the center to near the pin ends. This pattern was used to study the internal-tension-strain variations along the length of the specimen. The gages near the center of the specimen, top and bottom, were used to determine symmetry of the strains in the beam as the deflection went through a complete cycle and also were used to time correlate the dynamic strains.

The electronic circuitry that was used to monitor and measure the dynamic signals from the gages is shown schematically in Figure 6, and a photograph is shown in Figure 7. The strain gage was used as a variable resistor whose resistance change was a function of the elongation applied to the gage. A voltage of seven volts D.C. was applied to the gage from a 300-volt D.C. power supply through a variable 10k-Ohm dropping resistor. Analysis of the circuitry shows that not only was this a voltage-dropping resistor, but it was also a high impedance source to the A.C. signal coming from the strain gage. The signal was applied to the input of an A.C. amplifier (Eico, Model 250) which had a high impedance to the D.C. portion of the signal, allowing only the A.C. component to be amplified. From the output of the amplifier the signal was supplied to various instruments. The voltmeter (Hewlett-Packard Model 400H) and oscilloscope (Tektronix Model 503) were used to monitor only one strain gage amplitude and wave shape, and the

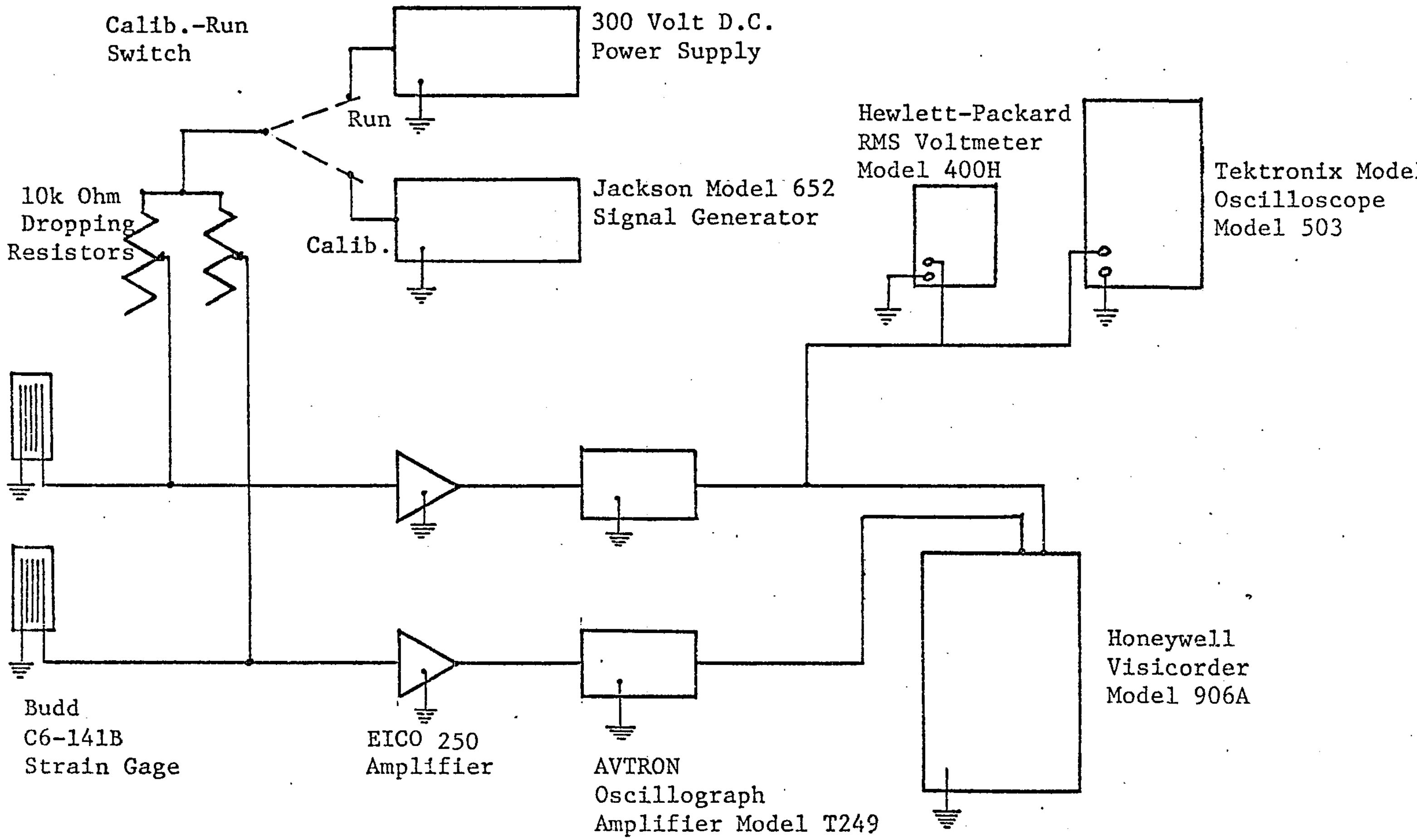

Note: Only two Strain-Gage Systems are shown.

STRAIN-GAGE ELECTRONIC SCHEMATIC DIAGRAM

FIGURE 6

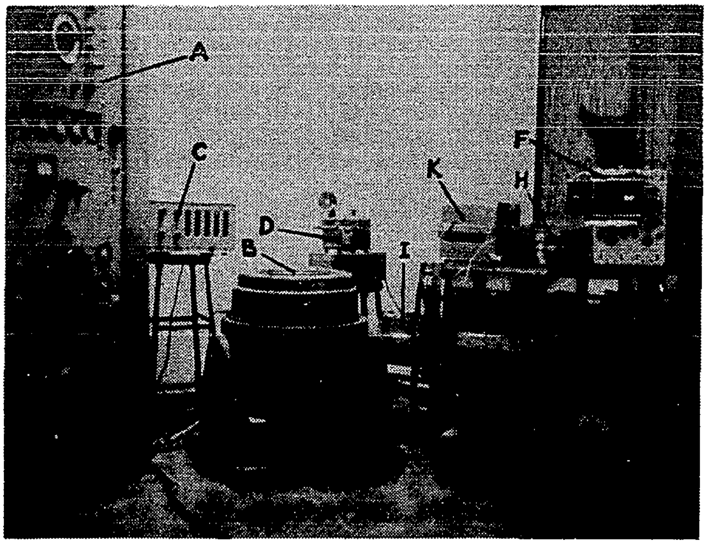

A. M-B ELECTRODYNAMIC EXCITER TABLE POWER SUPPLY: MODEL C-10

B. M-B ELECTRODYNAMIC EXCITER TABLE: MODEL C-10

C. CMC FREQUENCY COUNTER: MODEL 225B

D. GENERAL RADIO STROBOSCOPE: MODEL 1531-B

E. A.C. AMPLIFIERS: MODEL 250

F. TEKTRONIX OSCILLOSCOPE: MODEL 503

G. 300 VOLTS D.C. POWER SUPPLY

H. AVTRON OSCILLOGRAPH AMPLIFIER: MODEL T249

I. BUDD STRAIN GAGE INDICATOR: MODEL HW-1

J. JACKSON SIGNAL GENERATOR: MODEL 652

K. HONEYWELL VISICORDER: MODEL 906A

PHOTOGRAPH OF EXPERIMENTAL SYSTEM

FIGURE 7

outputs from all the gages were recorded on an oscillograph (Honeywell Visicorder Model 906A) through an oscillograph amplifier (AVTRON, Model T249) for a permanent record.

Calibration

Each strain-gage system was calibrated separately. A known sinusoidal signal was applied across each strain gage as indicated in Figure 6. With a known input amplitude, the signal was recorded on the oscillograph. The 300-volt D.C. power supply was removed when the systems were being calibrated. With the system calibrated in this manner, errors in the absolute strain values were minimized.

Frequency Response

The frequency response of the amplifier recording system has a flat response from 10 cycles per second (cps) to 25,000 cps; the range of this experiment was from 50 cps to 500 cps. The response of the strain gages for dynamic measurements were not measured in this test, but according to reference [27] the response is from 0 to 20,000 cps.

Dynamic Strains

The equation for the strain measurements taken from the strain gage system is [28]:

$$\text{G.F.} = (\Delta R/R)/(\Delta L/L)$$

where G.F. = gage factor

ΔR = change in gage resistance

R = gage resistance

ΔL = change in gage length

L = original gage length.

Therefore,

strain = $\varepsilon = (\Delta R/R)/(G.F.)$.

Analysis of the electronic circuitry (Figure 6) indicates that

$$(\Delta R/R) = (\Delta V/V)$$

where ΔV = change in voltage across the gage,

V = D.C. voltage across the gage,

therefore,

$$\varepsilon_d = (\Delta V/V)(G.F.)$$

where ε_d = dynamic strain.

The voltage change was taken from the strain-gage time history recorded on the oscillograph, after applying the appropriate calibration factor. Substitution into the above equation gave the dynamic strain values.

Test Procedure

The test procedure followed for the experiments was to obtain the highest frequency that would resonate the beam in a given mode for a preset maximum deflection and a preset initial tension on the beam.

The initial tension was applied to the beam without any dynamic load applied to the system. The output of one of the gages, usually the one closest to the pin end, was monitored on a strain gage indicator (Budd, Model HW-1) while the initial tension was being applied to the beam. The two set screws on the adjustment block were tightened only a few turns at a time to minimize the twisting on the beam.

The desired deflection of the beam vibration was set by adjusting the height of the pointed screw on the sliding block. Knowing the height of the beam in its undeflected position and the height of the adjusting screw, the relative deflection was readily determined.

Once the initial tension and relative deflection were set, the beam was set into vibration by the electrodynamic exciter. The peak resonant frequency for a given relative deflection was determined by slowly sweeping the resonant frequency range and noting the difference between the bottom of the beam and the top of the pointed screw on the sliding block. The stroboscope was used to "stop" the beam at its lowest point so that the relative deflection could be observed. The input frequency was increased slowly through the resonant condition many times, each time re-adjusting the input amplitude until the beam vibrated at the desired level.

When the desired level was reached, the strain-gage outputs were recorded on the oscillograph and the frequency was recorded from the frequency counter (Computer Measurements, Model 225B).

After the resonant frequency-amplitude point was recorded, the amplitude was changed and the procedure repeated. The same procedure was repeated while varying the amplitude ratio (a/h) from one to sixteen. Two initial strain values were used; 100 micro-inches per inch and 40 micro-inches per inch.

For the first mode the maximum amplitude was limited by the stress in the beam; the other modes were limited by the maximum-force output of the exciter.

Figures 8 and 9 show photographs of the beam in vibration.

Figure 8 shows the beam vibrating in the first mode at various amplitudes, and Figure 9 shows the beam vibrating in the third mode.

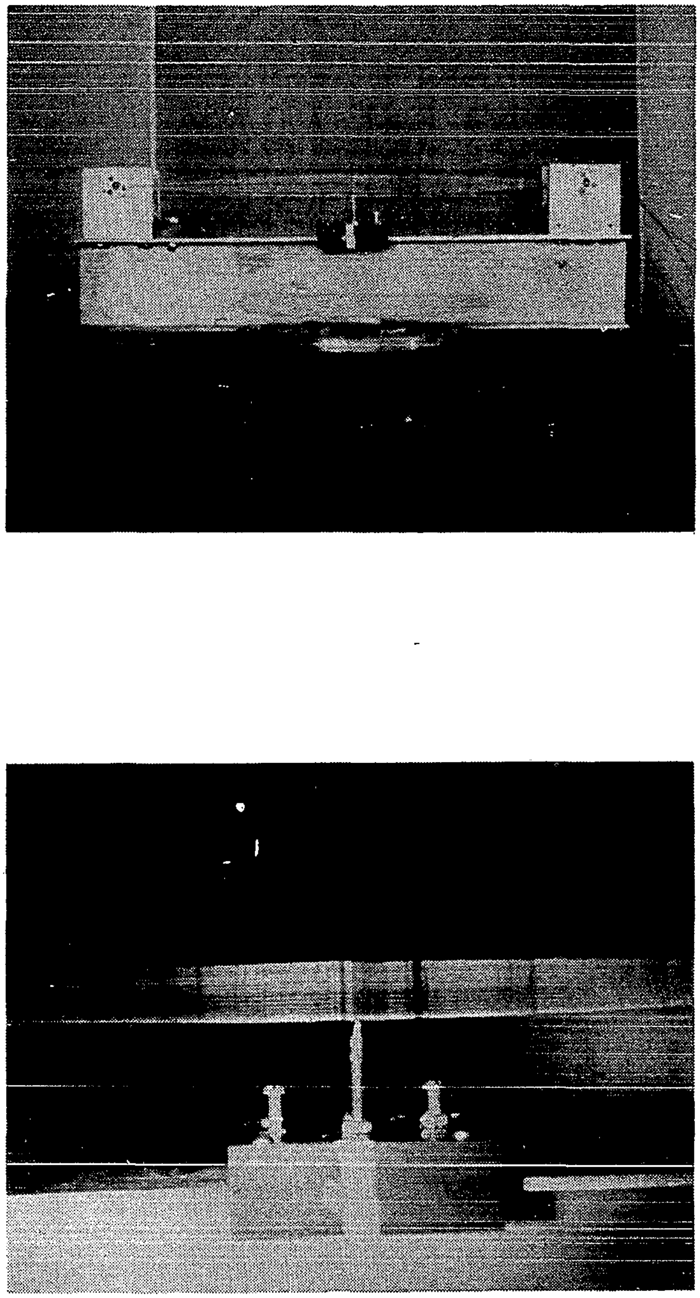

PHOTOGRAPHS OF SPECIMEN EXCITED IN FIRST MODE

FIGURE 8

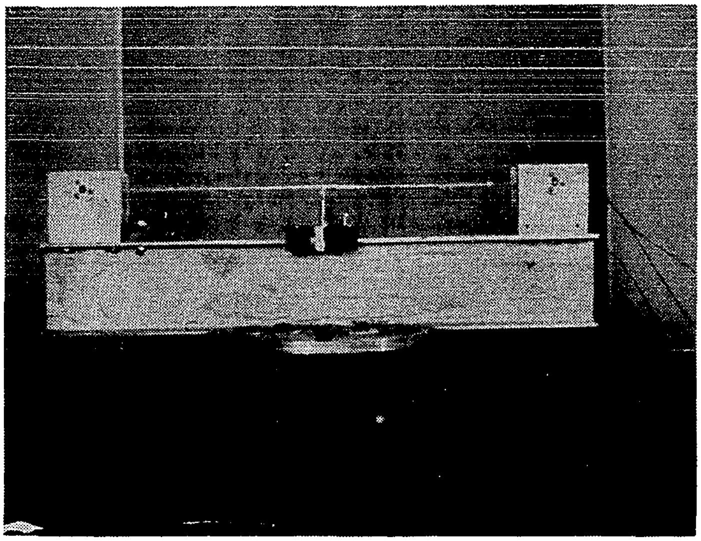

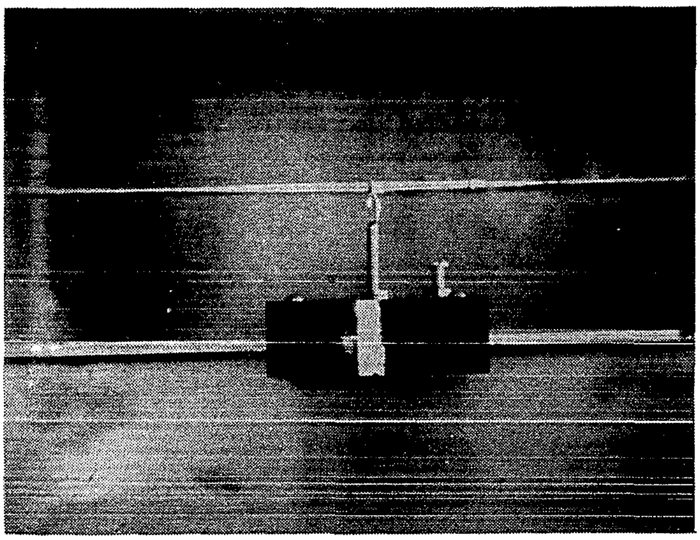

PHOTOGRAPHS OF SPECIMEN EXCITED IN THIRD MODE

FIGURE 9

CHAPTER IV

RESULTS

Introductory Remarks

The objectives of this investigation were established in the introduction. The experiments as outlined in Chapter III were designed to investigate system behavior as a function of the maximum amplitude of beam displacement. In this chapter a comparison is made between the experimental results and those established by the theoretical analyses. The following characteristics were investigated:

(a) resonant frequencies

(b) longitudinal stress

(c) modal shapes

(d) waveform

(e) damping.

Resonant Frequencies

Shown in Figures 10, 11, and 12 are plots of the resonant frequency of the specimen as a function of amplitude ratio. On each figure the curves were derived from the three methods developed in the analyses section. A copy of the computer program and a portion of the data print-out used to generate the curves are presented in Appendix B. Although the program was capable of analyzing any number of modes, only

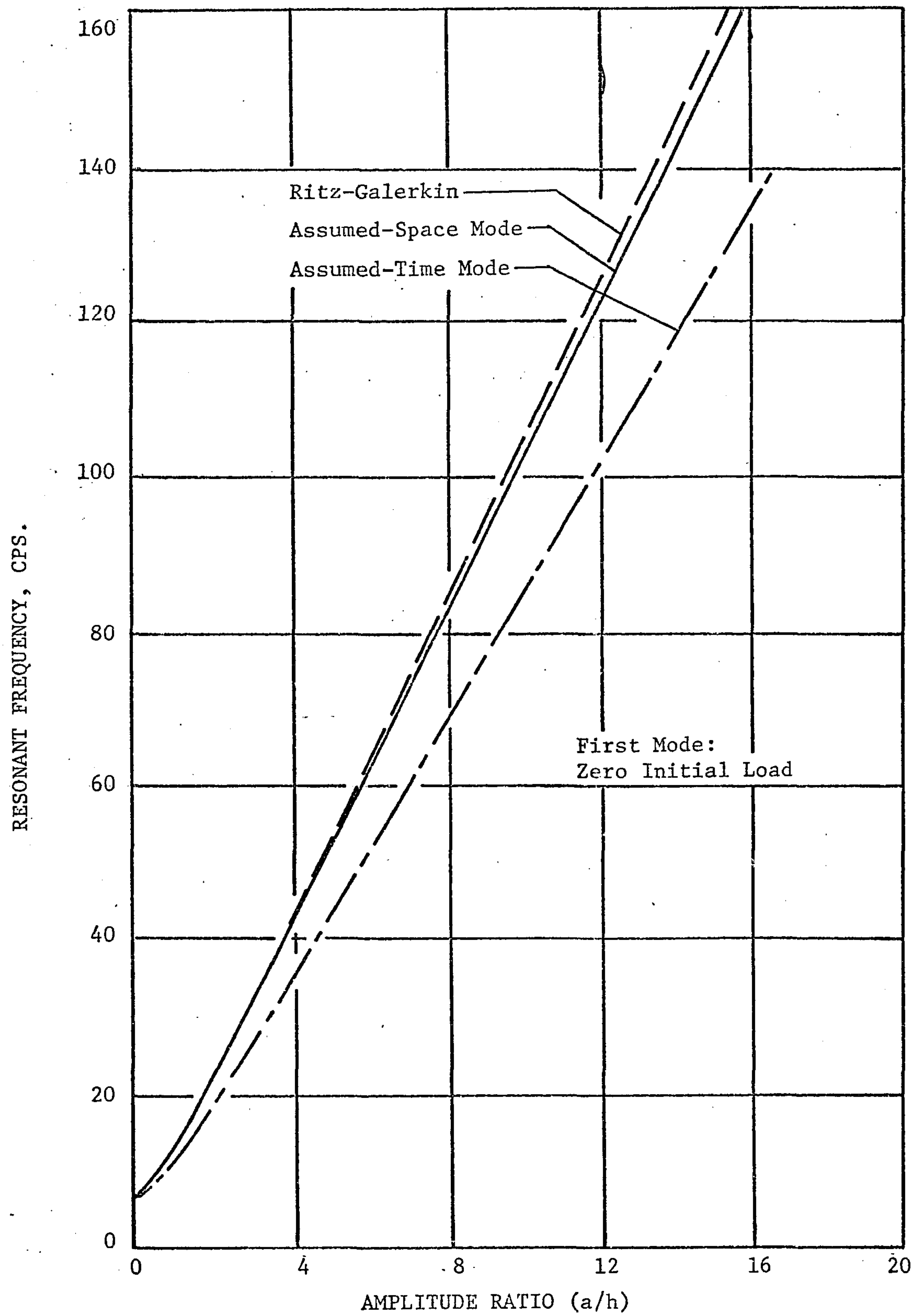

COMPARISON OF THEORETICAL SOLUTIONS, FIRST MODE

FIGURE 10

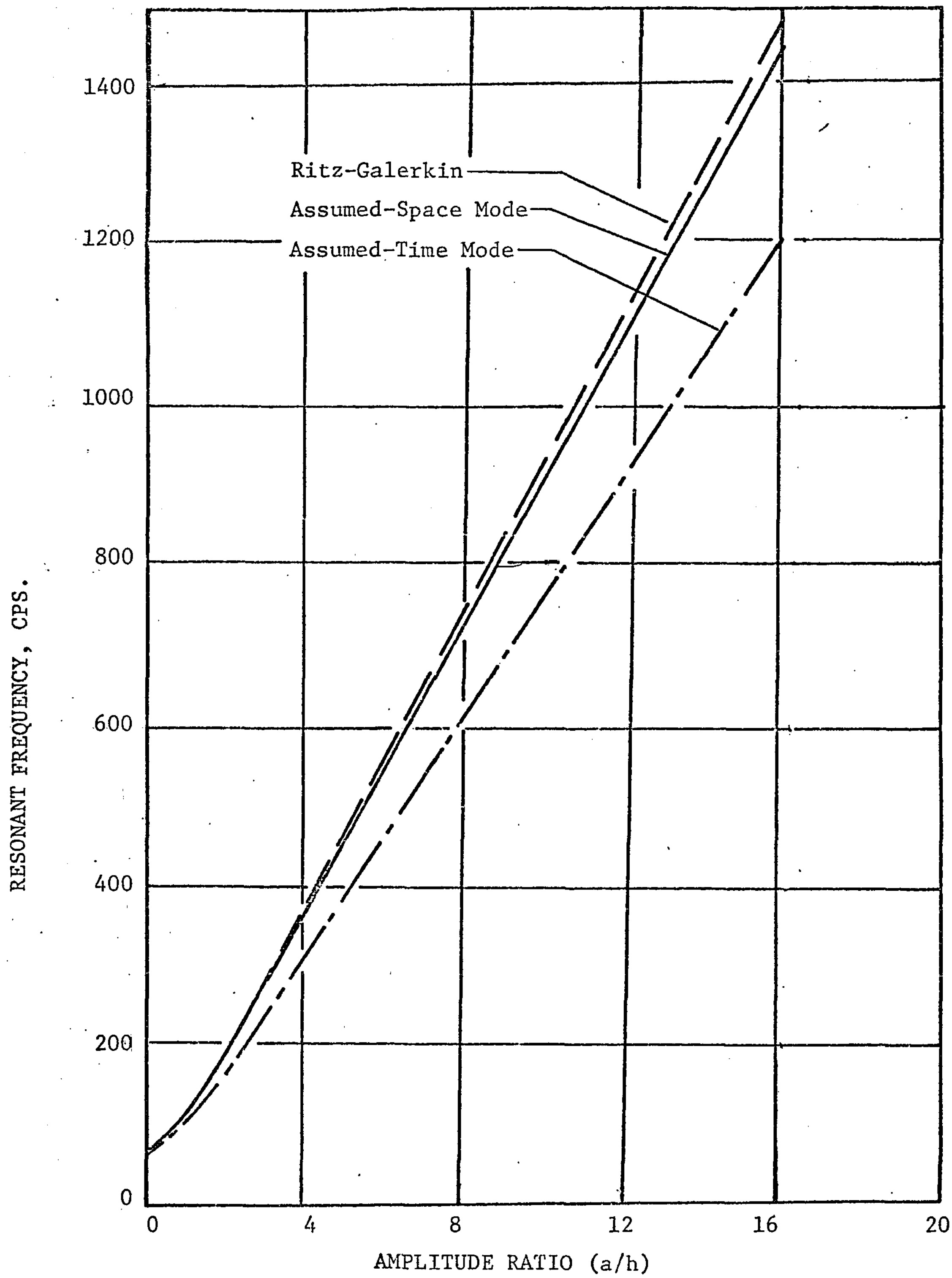

COMPARISON OF THEORETICAL SOLUTIONS, THIRD MODE

FIGURE 11

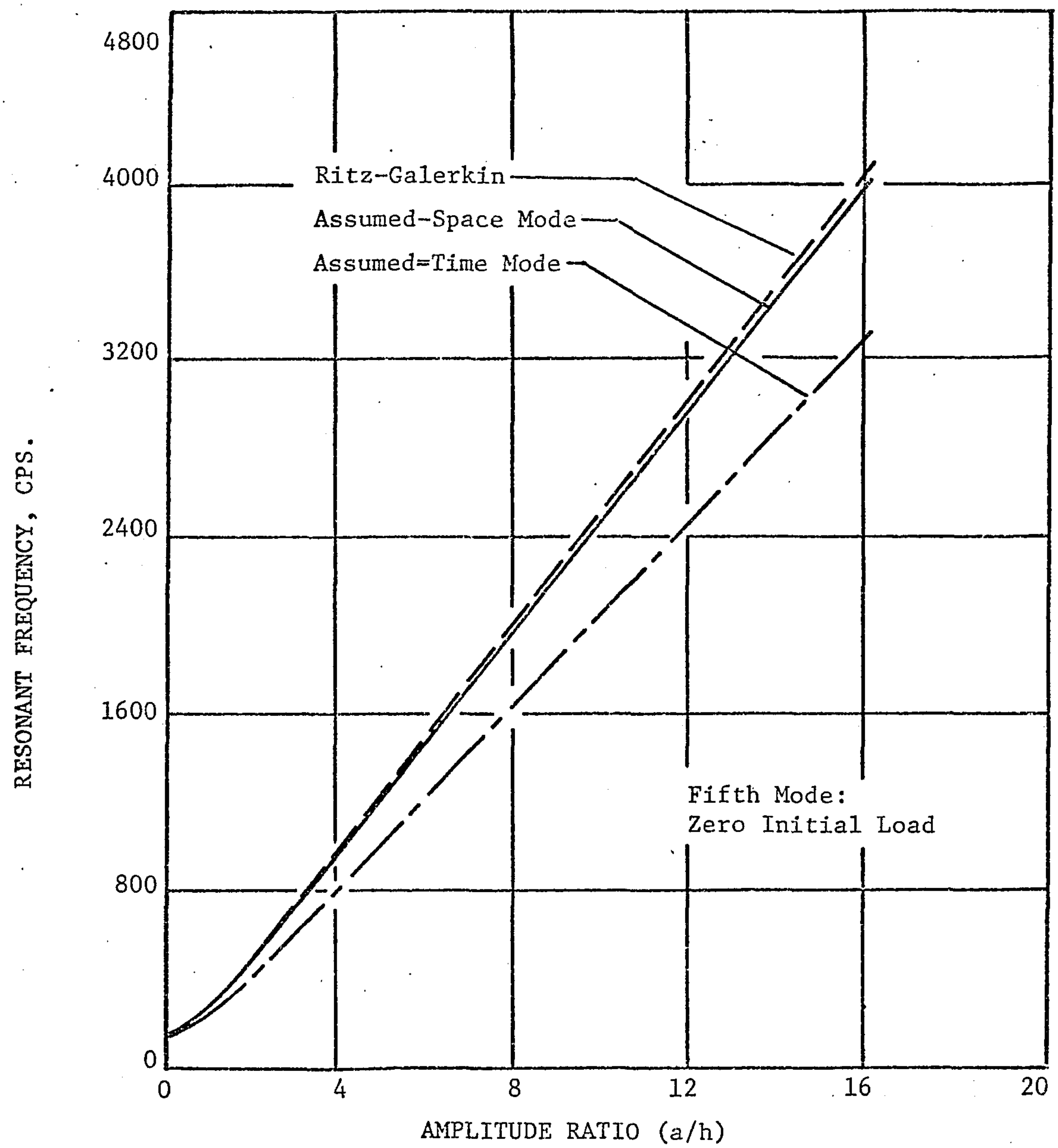

COMPARISON OF THEORETICAL SOLUTIONS, FIFTH MODE

FIGURE 12

the first, third, and fifth were computed. The higher modes were beyond the realm of this investigation and indicated the same trend as the lower modes.

The curves indicate that there is only a small difference between the resonant frequencies calculated by the Ritz-Galerkin and the assumed-space-mode methods of solution; the Ritz-Galerkin method gives slightly higher resonant frequencies than the assumed-space mode. The assumed-time mode method of solution indicates lower resonant frequencies than both the other methods. As indicated by the figures and the data print-out, the assumed-time mode method gives resonant frequencies 18% lower than the other methods.

As pointed out in Chapter II, the results obtained using Ritz-Galerkin, with a one-term approximation, were the same as the assumed-time mode when the third harmonic terms were deleted from the solution. On the figures, the Ritz-Galerkin curve is an indication of the results obtained from either method. This is done so that a distinction can be made between the two assumed-time-mode methods of solution, i.e. when the third harmonic terms are deleted and when the second harmonic terms are deleted.

Shown on Figures 13, 14, and 15 are curves indicating the change in resonant frequencies corresponding to the three modes as a function of amplitude ratio for various values of initial load. The curves show that at the lower amplitude ratios there is a separation between the resonant frequencies, but as the ratio increases, the curves tend to converge. As indicated on the figures, the convergence becomes asymptotic to an initial load line that is equivalent to the Euler column

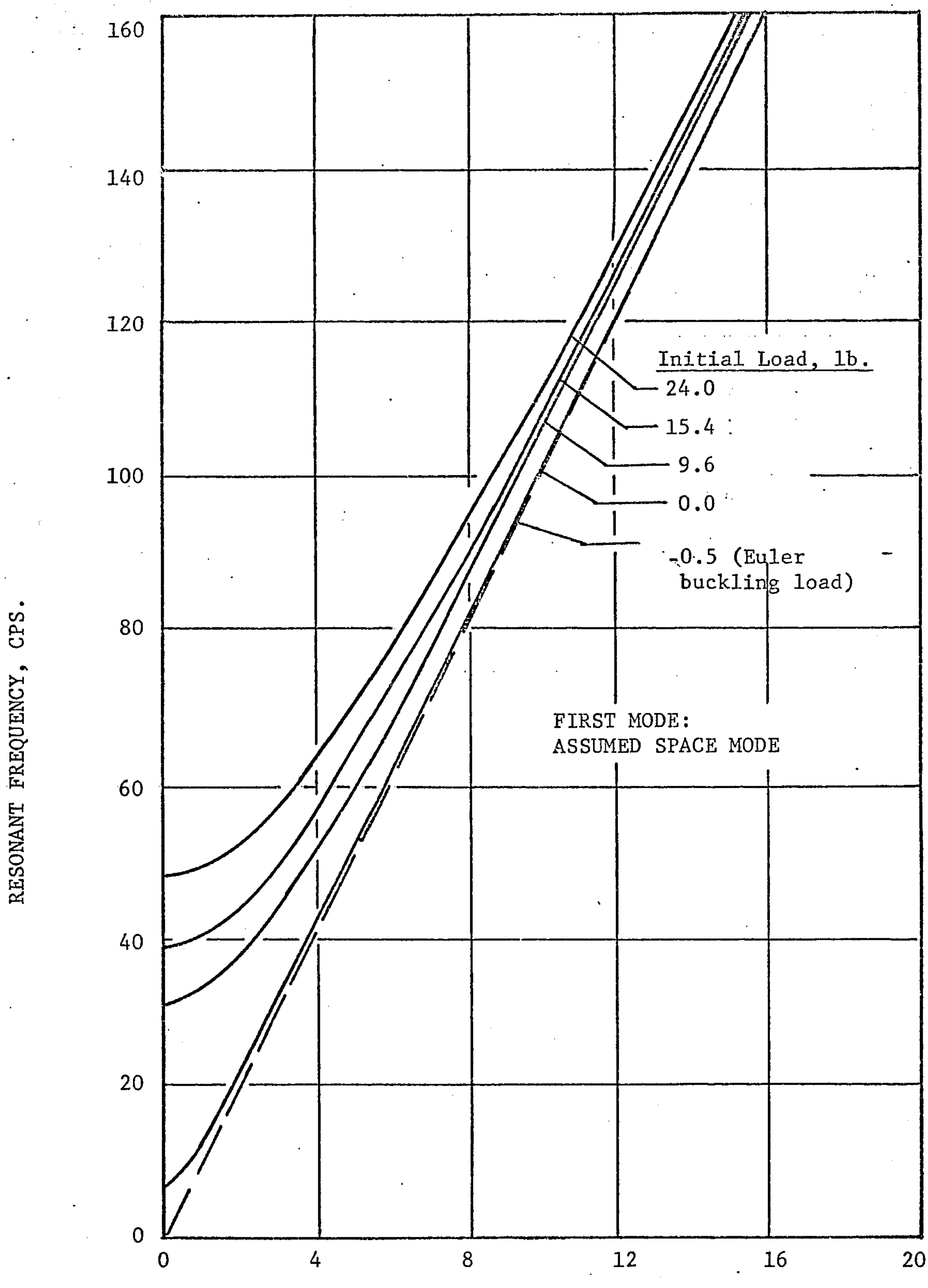

EFFECTS OF INITIAL LOAD, FIRST MODE

FIGURE 13

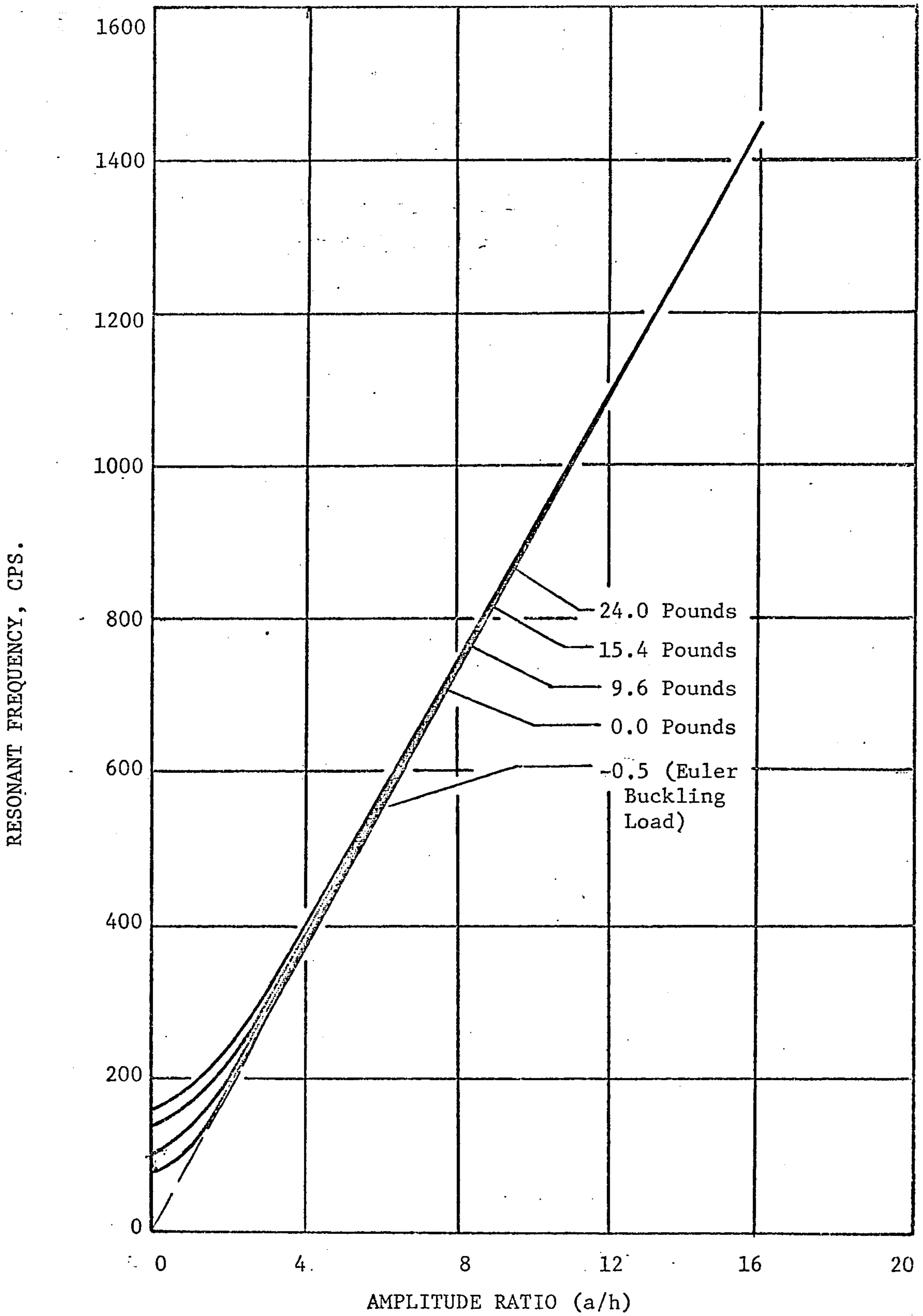

EFFECTS OF INITIAL LOAD, THIRD MODE

FIGURE 14

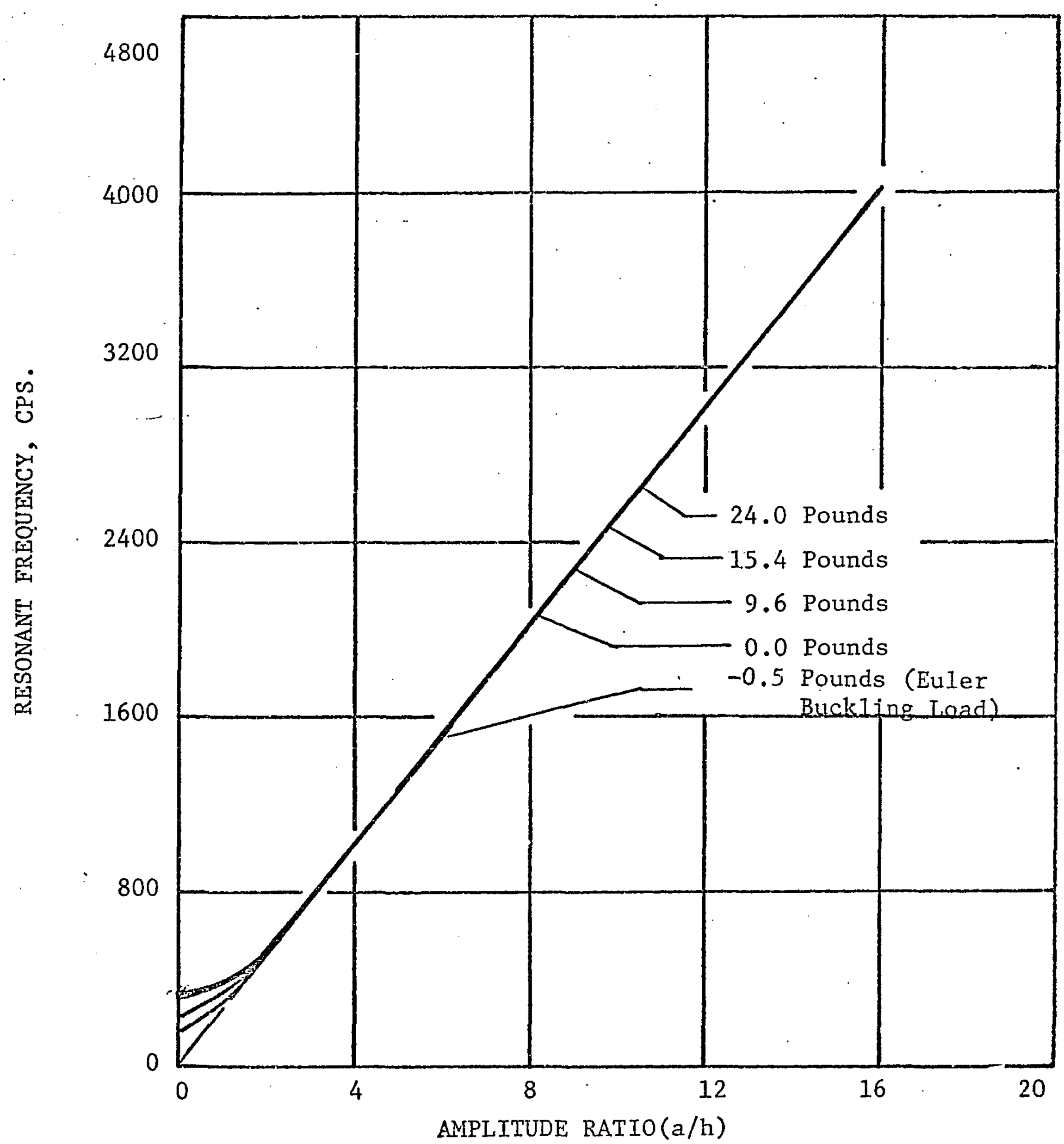

EFFECTS OF INITIAL LOAD, FIFTH MODE

FIGURE 15

buckling load (P_n). At this load, column buckling of the beam is impending and the above analyses are not valid.

Shown on Figures 16 and 17 is a comparison between the experimental data and the theoretical data. The experimental data were taken for two initial load conditions, 15.4 pounds tension and 24.0 pounds tension. For comparison, the data curves were separated for the two initial load conditions. Also shown on Figures 16 and 17 are plots of theoretical data modified to account for the flexibility of the shaft and support fixture under beam load. The development of these solutions are shown in Appendix A.

As can be seen by the curves, when the displacement of the shaft and blocks are included into the resonant frequency analyses, the agreement between the assumed-time mode and the experimental data are very good; the other methods still predict the resonant frequency to be higher than the experimental.

Some of the disagreement of the data at the higher ratio may be attributed to coupling between the modes. At the higher ratios there are common frequencies between the first and third modes at different amplitude ratios. This is in agreement with Srinivasan [15] using a two-term Ritz-Galerkin method of analysis.

There was also a noticeable "beat" phenomenon in the system when the exciting frequency was close to resonant. This is explained in reference [29] as a synchronization or "entrainment of frequency". In a forced nonlinear system when the exciting frequency approaches a resonant frequency, the two frequencies will beat together up to a certain frequency ratio at which time one will entrain the other and

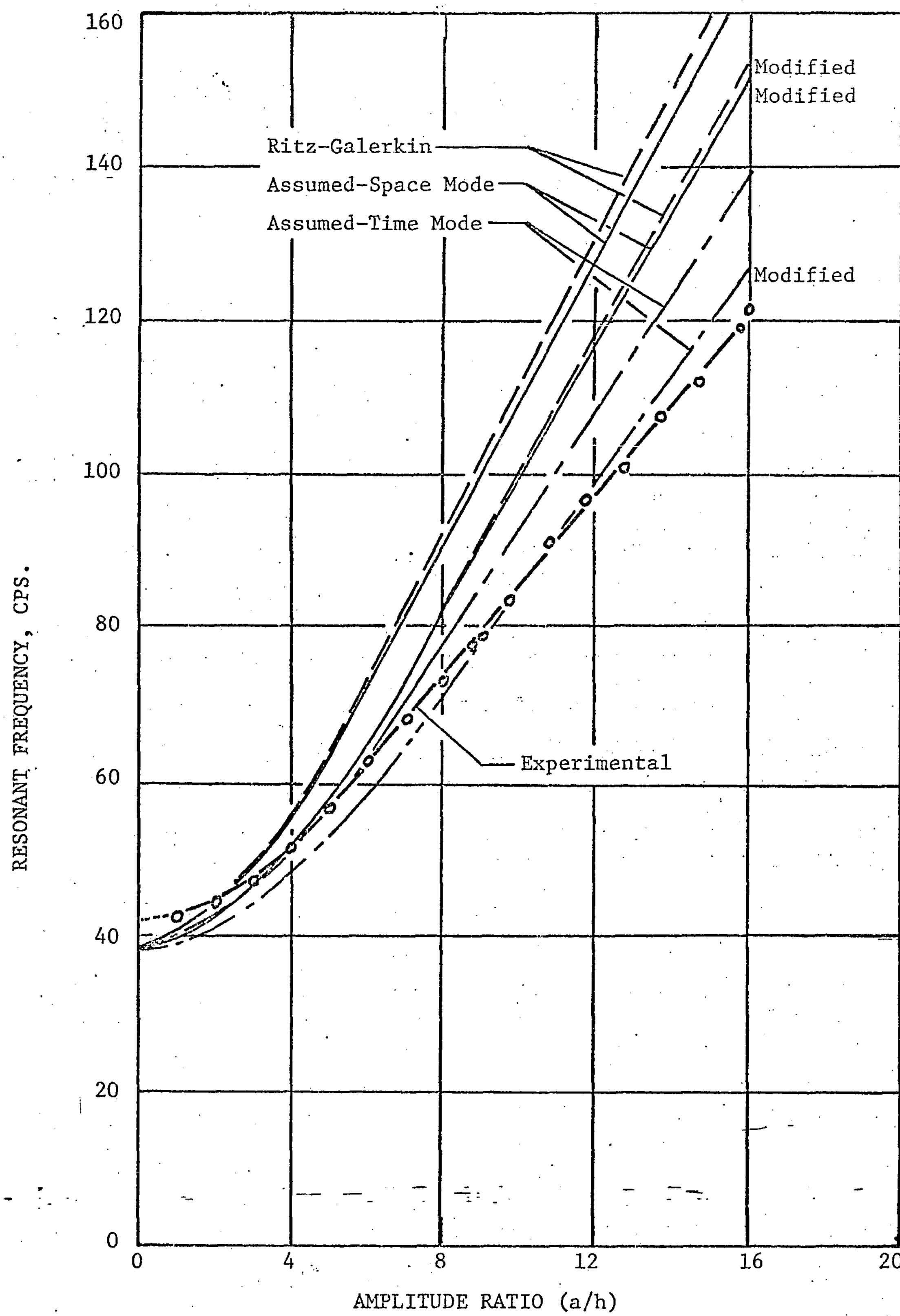

COMPARISON OF EXPERIMENTAL AND THEORETICAL DATA, N_o = 15.4 LBS.

FIGURE 16

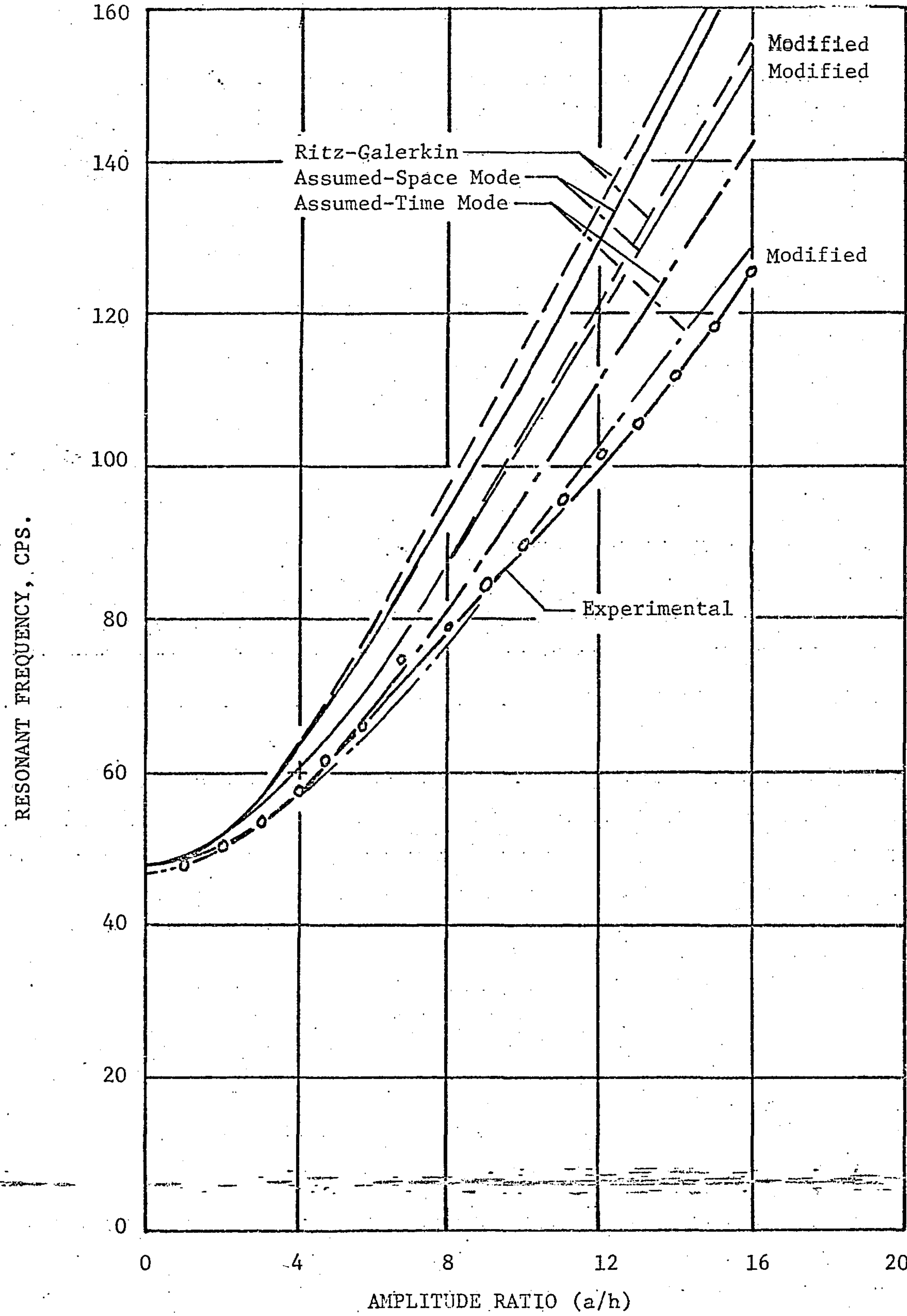

COMPARISON OF EXPERIMENTAL AND THEORETICAL DATA, N_o = 24 LBS.
FIGURE 17

the beating will disappear. This beating also could be a beating-traveling wave analogous to the ones mentioned by Williams [30]. Williams indicated an instability in disks above a certain amplitude that he accredited to beating traveling wave motion. The waves were due to a time phase between two preferential waves. This same phenomenon could have caused the beating in this experiment, because, as mentioned by Williams, slowly increasing the frequency into resonant (as was done in this investigation) a static modal pattern remains and the traveling wave will not occur.

Shown on Figure 18 is a comparison between some experimental data taken from investigations of Wah (5), Burgreen (8) and this investigation. Since the other investigators did not obtain data at the higher amplitude ratios (above 5), only the data for the common ratios are presented.

Another difference between the other experimental investigations and this one, was the method used to excite the system. In the other experiments the beam was held in an assumed mode and released, while in this experiment the system was base excited. When the beam is base excited, there is an additional term in the solution due to the base displacement. Shown in the Appendix A is the solution to the beam with base excitation. The base displacements that were measured in the experiments are shown on Figure 19 as a function of amplitude ratio. When these base excitation values were included in the theoretical analyses (equation 2D), there were negligible effects on the resonant frequency. Equation (2D) also implies that near the pin ends of the beam the resonant frequency will become zero or

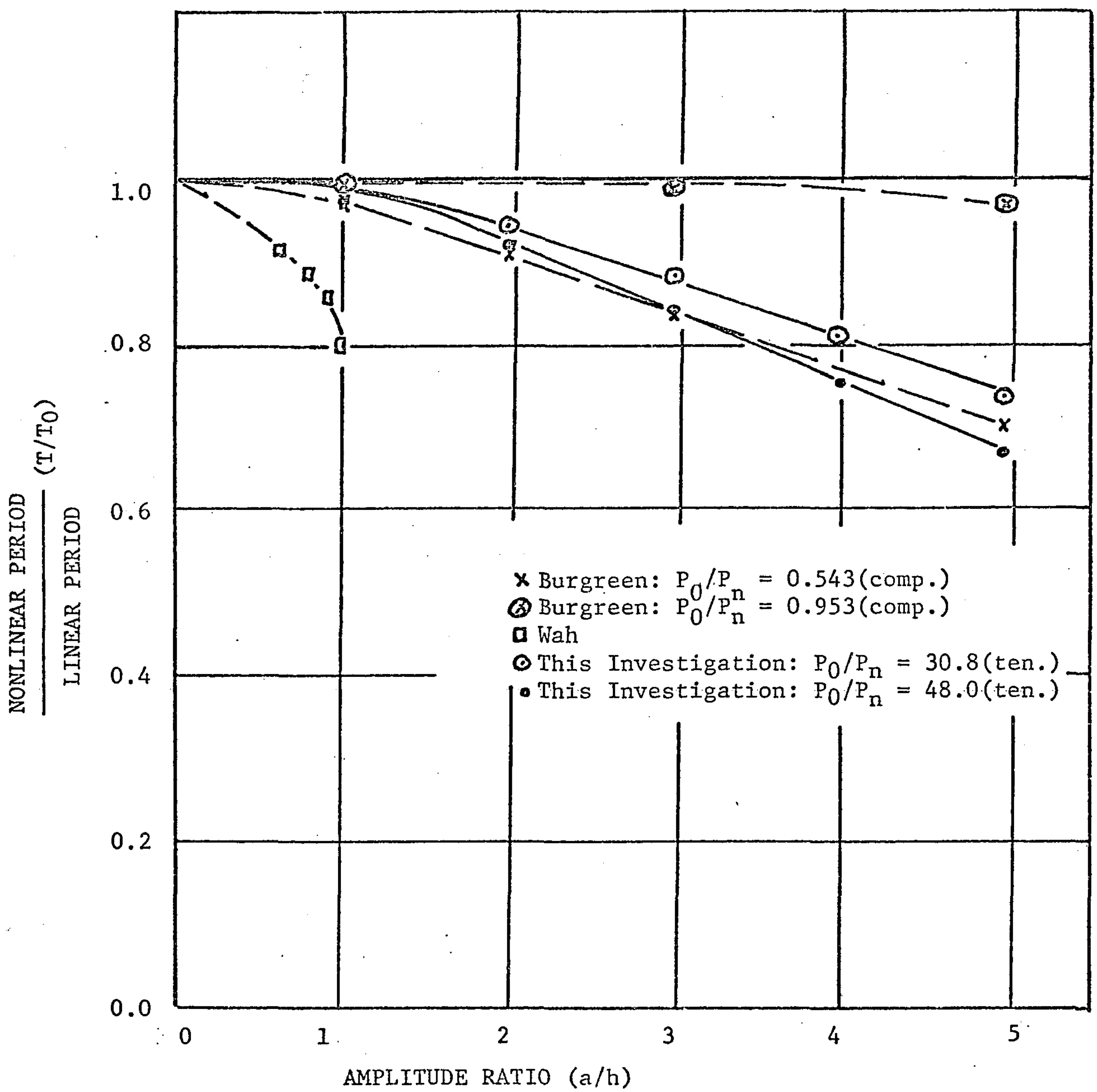

COMPARISON OF EXPERIMENTAL DATA WITH OTHER INVESTIGATORS

FIGURE 18

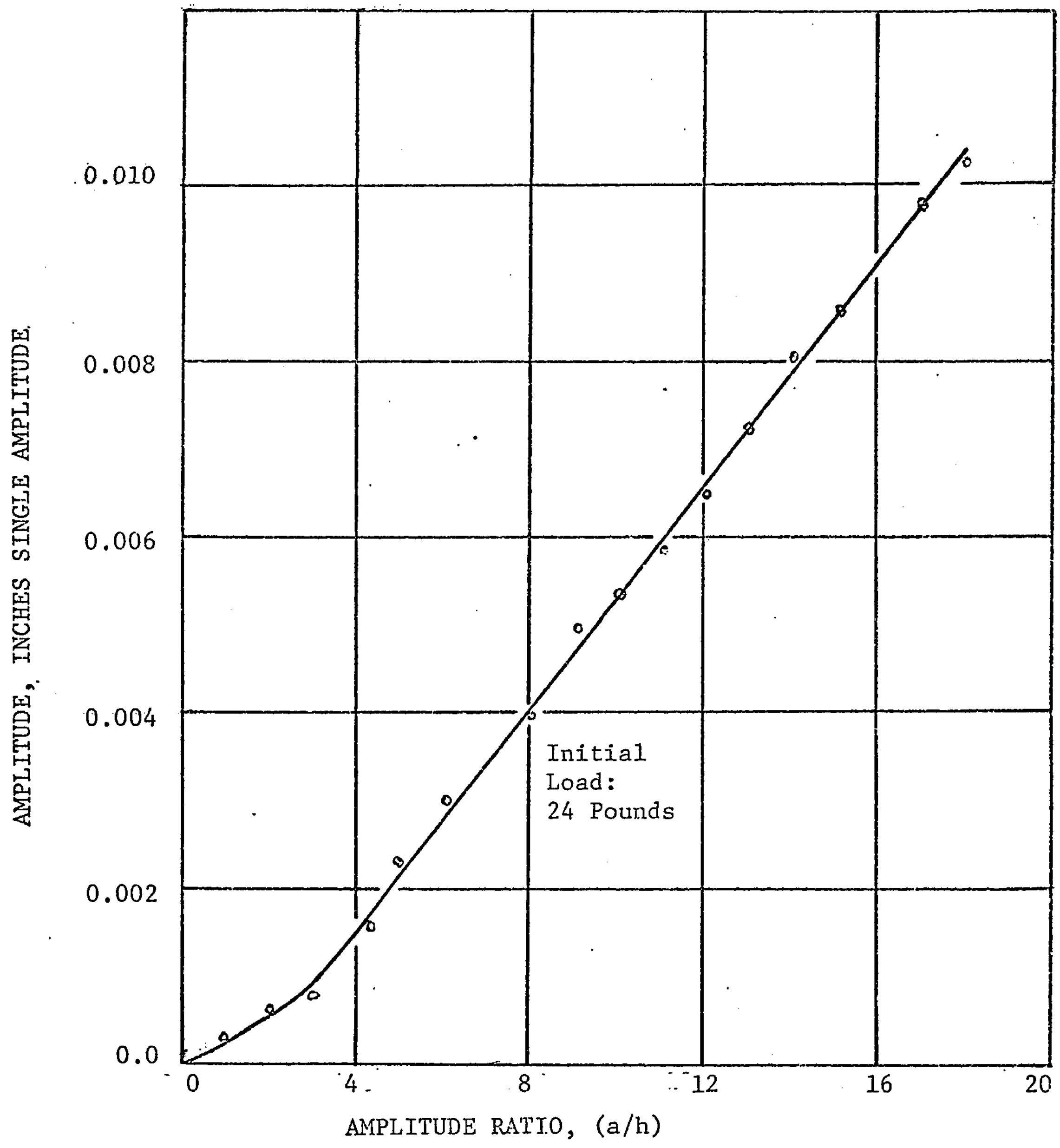

INPUT AMPLITUDE INTO VIBRATION SYSTEM

FIGURE 19

rigid-body motion, and at other points along the beam the resonant frequency will vary. This variation was checked by sweeping the resonant frequency range and observing the output of the gages along the beam. There was no noticeable change in resonant frequency along the beam. Calculations indicate that the gages were far enough from the ends so that any change in resonant frequency could not be detected on the gages. At the gage closest to the pin there would be a maximum of 5% variation in frequency.

When the equation of motion was derived, assumptions were made on the basis of the physical system. The following is a verification that the assumptions were valid:

(a) Small angle assumption

The angle of rotation for the first mode was largest at the pin end while the beam was undergoing its largest deflection. The maximum angle of rotation of five degrees was measured from the modal shape photograph using a protractor. This datum can be compared with theoretical value by differentiating the displacement function, v, with respect to x and maximizing the function; this gives the expression for the maximum angle of rotation at the pin ends as:

$$\theta_{max} = (a\, n\pi/\ell) .$$

When the values for maximum displacement, a, and beam length, ℓ, are substituted, the results yield

$$\theta_{max} = 6° \ 30' .$$

These values indicate a close agreement between the measured and calculated angle of rotation and they also indicate the validity of the small angle assumption:

$\sin 6° 30' = 0.1132$, and $6° 30' = 0.1134$ radians.

From this, the assumption that θ^2 is small compared to unity is valid: i.e. $(1 + \theta^2) = (1 + 0.012) \approx 1$

(b) Rotatory Inertia and Shear Deformation

Anderson [31] indicated that for an (r/ℓ) ratio below approximately 0.1, rotatory inertia and shear deformation have no effect on the linear resonant frequency of a simply-supported beam. The (r/ℓ) ratio for this investigation was 25×10^{-5}.

Test data are presented on the first and third modes only. Because of the exciter limitation, no data were obtained on modes above the third. Figure 20 shows the experimental and theoretical data obtained on the third mode. For the amplitude ratios investigated there was fair agreement between the theoretical and experimental data.

Longitudinal Stress

As pointed out previously, there were three major contributions to the longitudinal stress on the beam during vibration:

(a) Vibratory bending

(b) Vibratory stretching

(c) Static initial tension.

Test data results taken from the gages equally spaced along the beam were used to investigate the stress distribution.

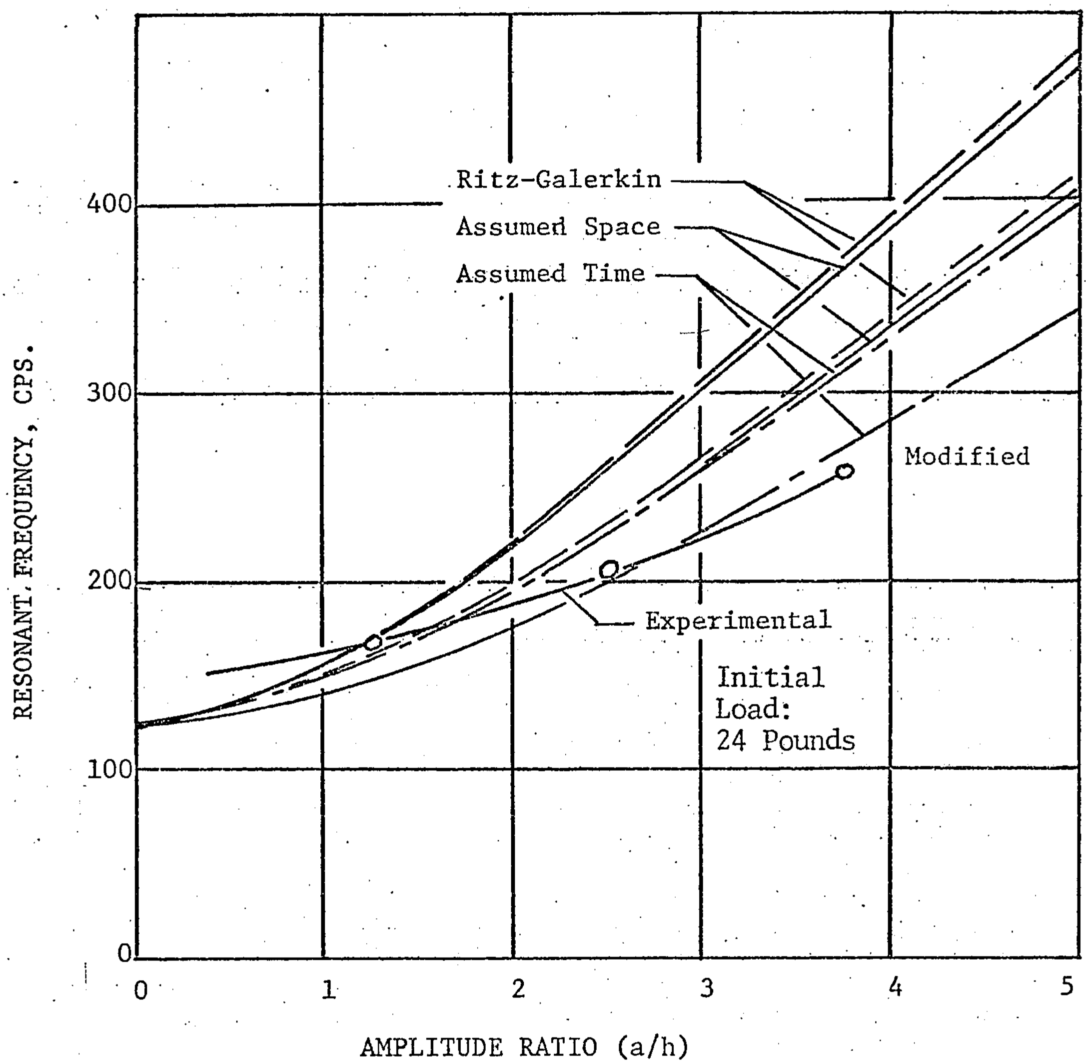

COMPARISON OF EXPERIMENTAL AND

THEORETICAL DATA, THIRD MODE

FIGURE 20

Figure 21 is a copy of an oscillograph record which indicates the strain at the various gage locations. The signal from the gage closest to the pin end indicates a sinusoidal wave that is one half the period of the other waves. Since this gage is exposed to a minimum amount of bending, it should conform to the stretching strain on the beam. The gage in the center of the beam, which should indicate the maximum bending strain, shows a complex waveform. Figure 22 shows a photograph of this waveform taken with an oscilloscope camera (Tektronix Model No. 503 with camera attachment Model No. 125). Fourier analyses were carried out on this wave and the major frequency components of the equation are shown on Figure 22. The main components were a sine wave superimposed on a sine squared wave [$\sin^2 \omega t = (1/2)\ (1 - \cos 2\omega t)$] and an additional $\sin 2\omega t$ component.

The sine wave is the bending strain, the sine squared wave is the stretching strain, and the $\sin 2\omega t$ wave is due either to the unsymmetrical wave form or the hysteresis damping that occurred when the material was stretched.

From the oscillograph records, the maximum strain caused by the bending was subtracted from the maximum data value at each gage location which left only the maximum strain due to stretching. These data are shown on Figure 23 and indicate that the maximum stretching strain across the beam was constant. These data validate the assumption that there was no change in the stretching force across the beam. The remaining bending strain is shown on Figure 24.

The stretching strain as a function of amplitude ratio is shown on Figure 25. On this figure is a comparison of the experimental and

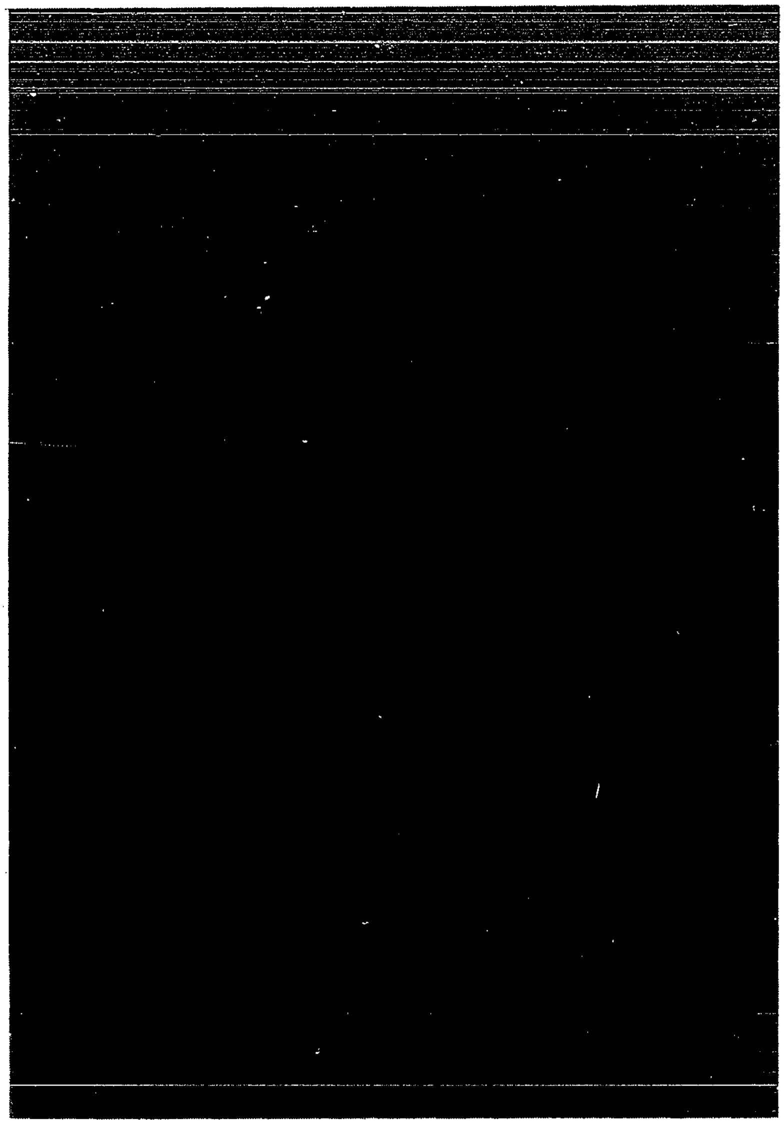

OSCILLOGRAPH RECORD

FIGURE 21

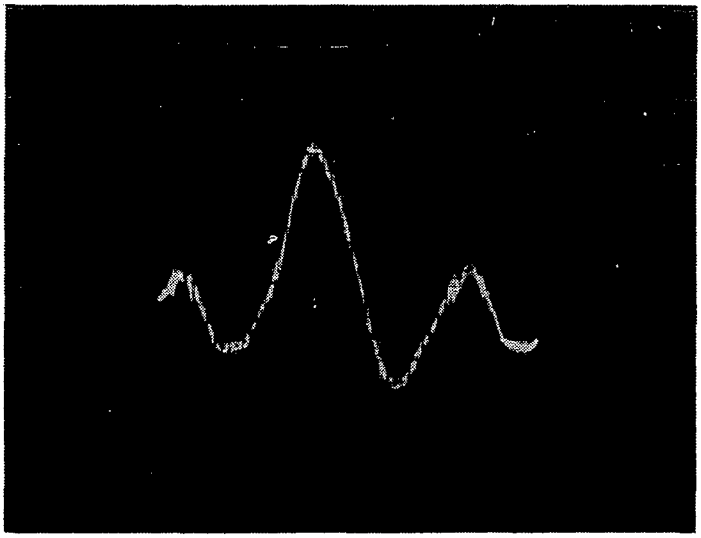

$$v = 1.10 \sin \omega t - 0.42 \sin 2\omega t + 1.0 - 1.3 \cos 2\omega t$$

WAVEFORM

FIGURE 22

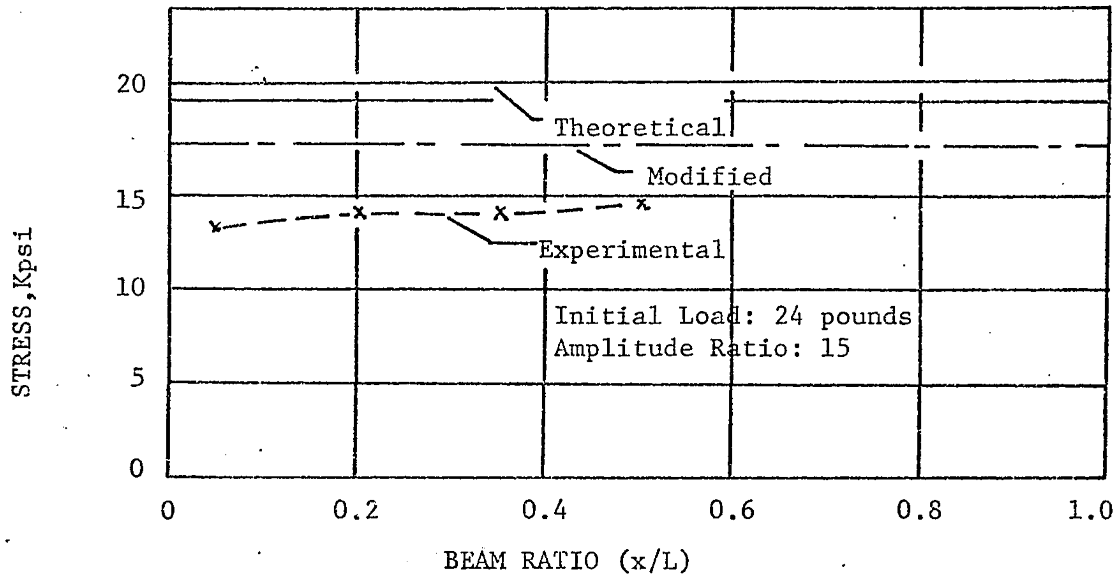

STRETCHING STRESS ACROSS BEAM

FIGURE 23

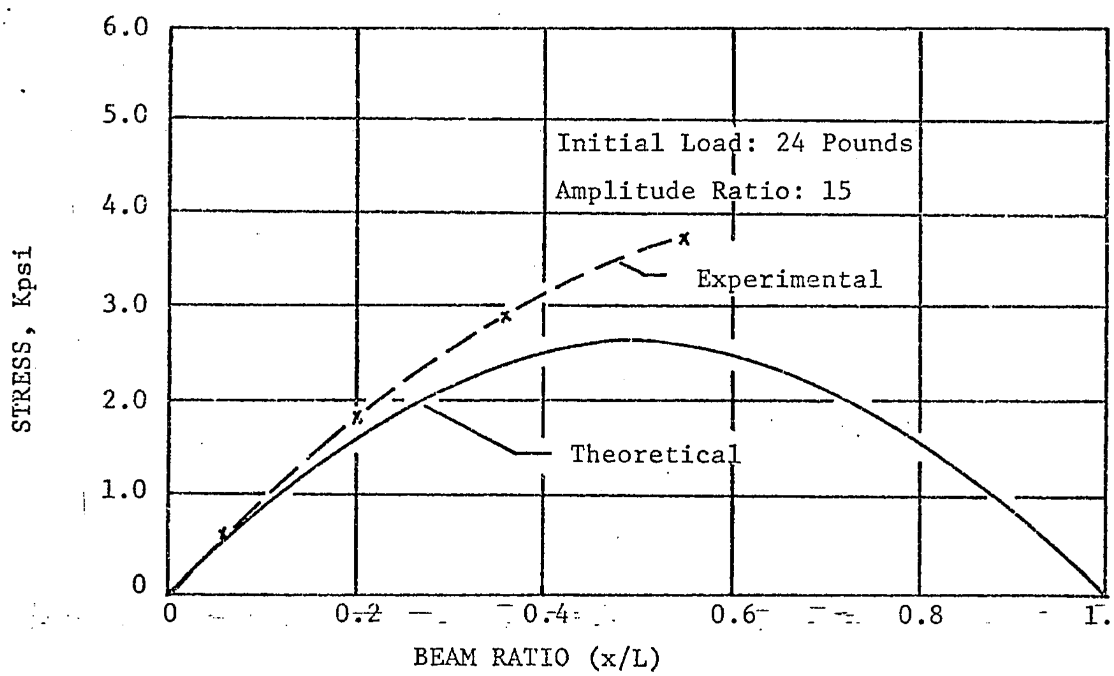

BENDING STRESS ACROSS BEAM

FIGURE 24

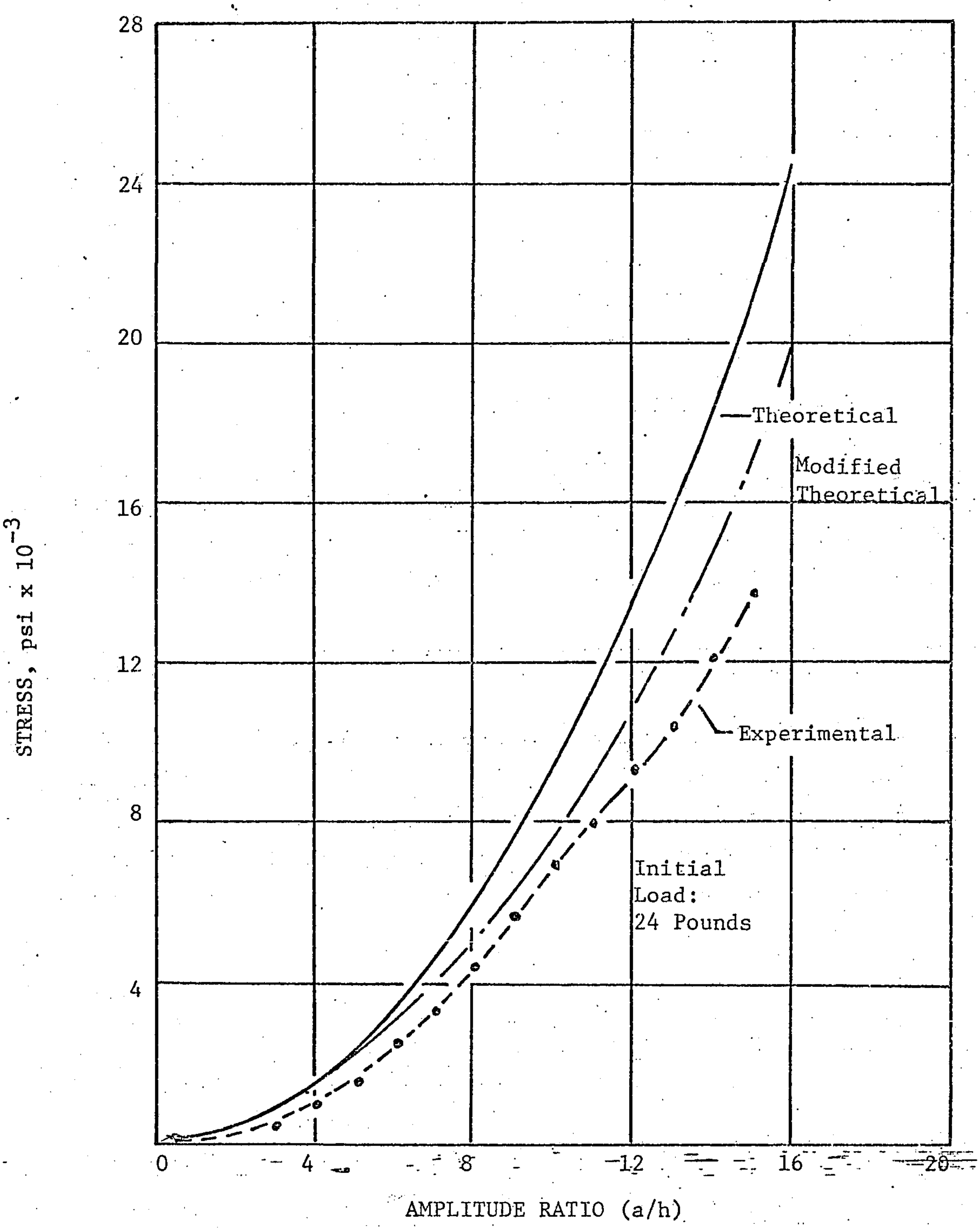

STRESS DUE TO STRETCHING

FIGURE 25

theoretical values. As can be seen by the curves, the experimental data did not agree well with the predicted. The difference may be attributed to many things, the major one being the flexibility of the shaft and fixture that held the experimental beam. The analyses can be modified to account for the flexibility of the shaft and fixture as shown in Appendix A. Shown on Figure 25 is the plot of the stretching stress as a function of amplitude ratio, modified to account for the flexibility. With this modification, the agreement is good.

Other factors that could effect the strain experienced by the strain gage is a frictional moment applied to the beam by the bearings. This moment would apply a slope to the beam in opposition to the rotation slope and reduce the strain on the upper fibers. The strain would be applied at the same frequency as the stretching strain.

Modal Shape

Shown on Figure 26 are plots of the space modal shape of the beam, comparing the experimental with the theoretical (see equations 44 and 62) at maximum amplitude. The experimental modal shape was taken from a close-up photograph of the beam in vibration. The stroboscope was used to "stop" the beam's motion.

As can be seen from the curves, the experimental modal shape agreed closely with the theoretical within the experimental accuracy.

Waveform

Shown on Figure 27 are plots of the waveform of the beam's

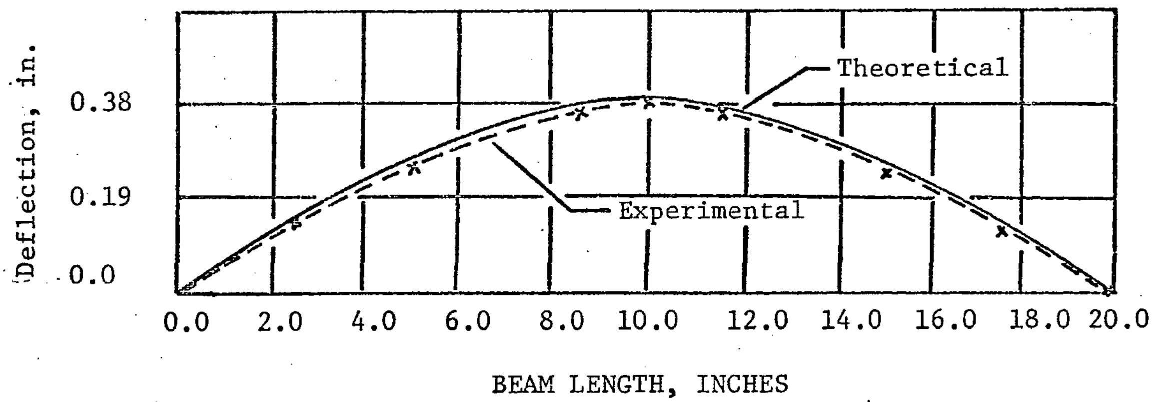

COMPARISON OF SPACE MODAL SHAPE

FIGURE 26

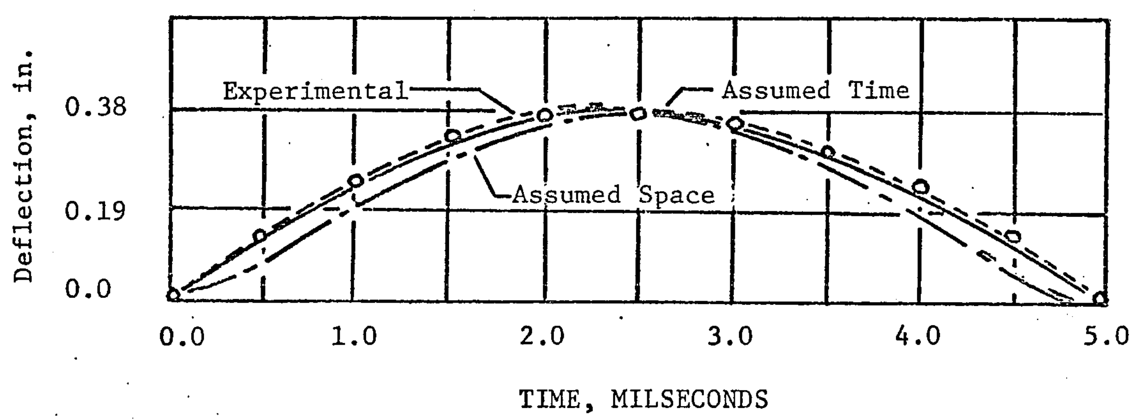

COMPARISON OF TIME MODAL SHAPE

FIGURE 27

center, comparing experimental with theoretical at the maximum amplitude ratio. The experimental was taken from the oscillograph records at equal time intervals. As can be seen on the figure, there was little difference between the experimental and theoretical waveforms when the assumed-time mode or Ritz-Galerkin method of solution was used ($v = a \sin \alpha x \sin \omega t$), but a greater difference is noted when the assumed-space mode method of solution is used [$v = a \sin \alpha x \, \mathrm{cn}\,(pt, k)$].

Damping

Damping was investigated experimentally at various amplitudes of excitation. The beam was excited at the amplitude and then an oscillograph record was taken on the strain decay. Log decrements were calculated from the oscillograph record. Figure 28 shows a plot of the log decrement as a function of amplitude ratio and position along the beam. The damping obtained was the effective damping of the system due to the stretching strain, bending strain, bearing friction, and air damping.

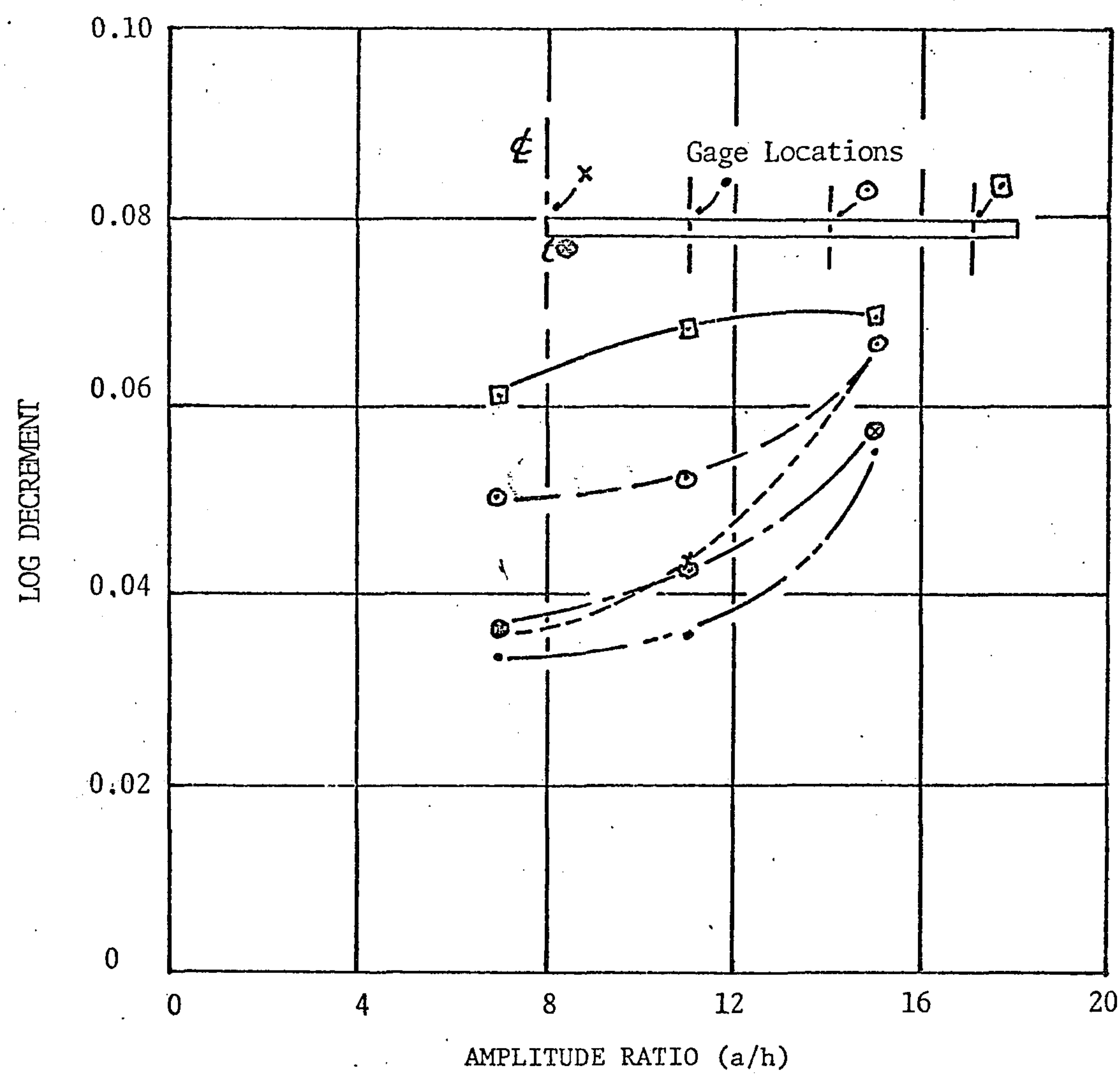

LOG DECREMENT VARIATION

FIGURE 28

CHAPTER V

CONCLUSIONS

Concluding Remarks

The data derived from the experimental investigation agreed in most aspects with the theoretical data that were generated for the special case. The objectives of this investigation were directed toward examining the limitations of existing theory of nonlinear vibrating continuous systems. Within the special case of the simply-supported pin-end beam the normal modes were separable, but there was coupling that distorted the theoretical analyses at large amplitude ratios. Not only did this distortion exist in the resonant frequencies, but also in the stretching strain and the modal shapes. In reviewing the theoretical analyses, such coupling might be expected since there are common resonant frequencies between the different modes although the amplitude ratios were different. This would cause a coupling between modes and further this coupling would cause an effect on the strain and modal shapes. The limitation of the instrumentation that was used in this investigation did not allow the detection of the minor mode or modes as the case may have been. An indication was noted visually that coupling was present by the response of the beam during maximum deflection.

It is the conclusion of this investigation that all the methods of solution that were developed for a simply-supported pin-ended beam are applicable up to an amplitude-ratio of approximately five, but beyond this point the assumed-time mode method of solution gives the best results. When there are coupling of modes, the amplitude of each contributing mode would need to be known before a comparison of the theoretical and experimental could be made. The superposition theory is valid in the separation of modes, but the coupling effects between modes need to be considered in the final results.

Recommendations for Further Research

Additional investigations need to be made to further answer the question of the extent that coupling affects the results of existing theory. This could be done by analyzing the transducer signal with a higher degree of accuracy in an effort to detect the existence of higher modes and to relate this analysis with the theory. Additional investigations could be made to determine the effective damping caused by the stretching of the beam under deflection.

This investigation dealt with the simply-supported pin-ended beam only. A similar type of investigation could be made on beams with other boundary conditions. The thickness, which would include shear deformation and rotatory inertia, could be investigated to further advance the knowledge, however, much needs to be done to understand the basic theory before the general cases are attempted.

REFERENCES

1. W.F. Ames, "Nonlinear Partial Differential Equations in Engineering." Academic Press, New York, (1965).

2. S.E. Jones and W.F. Ames, "Nonlinear Superposition." J. Math. Anal. and Appn. 17, 484 (1967).

3. R.M. Rosenberg, "On Nonlinear Vibrations of Systems with many Degrees of Freedom." Advances in Applied Mechanics. 9, 156, Academic Press, New York (1966).

4. T. Wah, "The Normal Modes of Vibration of Certain Nonlinear Continuous Systems." J. Appl. Mech. 31, 139, (1964).

5. T. Wah, "Theoretical and Experimental Investigations of Nonlinear Dynamic Response of Continuous Systems." Final Rpt. SWRI Project 03-1435, Southwest Research Institute, San Antonio, Texas (1965).

6. S. Woinowsky-Krieger, "The Effects of An Axial Force on the Vibration of a Hinged Bar." J. Appl. Mech., 17, 35 (1950).

7. P.H. McDonald, "Nonlinear Dynamic Coupling in a Beam Vibration." J. Appl. Mech., 22, 573 (1955).

8. D. Burgreen, "Free Vibrations of a Pin-Ended Column With Constant Distance Between Pin Ends." J. Appl. Mech., 18, 135 (1951).

9. J. Mayers and B.G. Wrenn, "Combined Influence of Higher Order Linear Effects and Nonlinear Effects on the Lateral Vibrations Behavior of Solid and Sandwich Beams." SUDAER No. 208, Stanford University, Dept. of Aeronautics and Astronautics (Sept. 1964).

10. S.R. Woodall, "On the Large Amplitude Oscillations of a Thin Elastic Beam." Int. J. Nonlinear Mech. 1, 217, (1966).

11. E.H. Dowell, "Nonlinear Oscillations of a Fluttering Plate." AIAA Paper No. 66-70 (Jan. 1966).

12. Y.Y. Yu and J.L. Lai, "Application of Galerkins Method to Dynamic Analysis of Structures." AIAA J. 5, No. 4, 792, (1962).

13. D.A. Evensen, "Nonlinear Vibrations of Beams with Various Boundary Conditions." AIAA J. 6, No. 2, 370 (1968).

14. A.V. Srinivasan, "Large Amplitude-Free Oscillations of Beams and Plates." AIAA J., 3, No. 10, 1951, (1965).

15. A.V. Srinivasan, "Non-Linear Vibrations of Beams and Plates." Int. J. Non-Linear Mech., 1, 179 (1966).

16. A.C. Eringen, "On the Non-Linear Vibration of Elastic Bars." Q. Appl. Math., 9, 361 (1952).

17. W.H. Warner, "The Dynamical Equations for Beams." Contract No. Nobs - 86783 Code 345, Bu Ships, U.S. Navy (1964).

18. H. Wagner, "Large-Amplitude Free Vibrations of a Beam." J. Appl. Mech., 32, 887 (1965).

19. E.J. Scott and D.R. Carver, "On the Nonlinear Differential Equation for a Beam Deflection." J. Appl. Mech., 22, 245, (1955).

20. J.H. Somerset and R.M. Evan-Ivanowski, "Influence on Non-Linear Inertia of the Parametric Response of Rectangular Plates." J. Non-Linear Mech., 2, 217 (1967).

21. J.G. Eisley, "Large Amplitude Vibrations of Buckled Beams and Rectangular Plates." AIAA J., 2, No. 12, 2207 (1964).

22. H. Lurie, "Lateral Vibrations as Related to Structural Stability." J. Appl. Mech., 19, 195 (1952).

23. G.V. Mishenkov, "On the Question of the Interaction of Parametrically Excited and Forced Vibrations of Elastic Panels." Izestiya Akademiya Navk Arm, SSR, 18, 53 (1965).

24. P.E. Wilson and A.P. Boresi, "Large Deflection of a Clamped Circular Plate Including Effects of Transverse Shear." J. Appl. Mech., 31, 540 (1964).

25. F.R. Arnold, "A Derivation and Application of Second Ritz Method to the Solution of Multi-Degree of Freedom Systems." Proc 9th Int. C. Appl. Mech., 7, 319 (1957).

26. "Air Weapons Materials Application Handbook, Metals and Alloys" Air Force Research & Development Command Rpt. TR 59-66 (1959).

27. R.C. Dove and P.H. Adams, "Experimental Stress Analysis and Motion Measurement." Merrill, Columbus, 226 (1964).

28. C.C. Perry and H.R. Lissner, "The Strain Gage Primer." McGraw-Hill, New York (1955).

29. N. Minorsky, "Nonlinear Oscillations." D. Van Nostrand, Prentice, 438 (1962).

30. C.J.H. Williams, "The Stability of Modal Patterns in Disk Vibration." Int. J. Mech. Sci., 8, 421 (1966).

31. R.A. Anderson, "Flexural Vibrations in Uniform Beams According to Timoshenko Theory." J. Appl. Mech., 20, 504 (1953).

32. A.P. Boresi, "Elasticity in Engineering Mechanics." Princeton-Hall, Inc., Englewood Cliffs, N.J. 69 (1965).

33. F.B. Seely, "Resistance of Materials." Wiley, N.Y., 2nd Edition, 121 (1935).

34. W.L. Hart, "Calculus." Heath, Boston, 318 (1955).

APPENDIX A

EQUATIONS OF MOTION FOR BEAM ELEMENT

The dynamic equilibrium equations of a simply supported beam are derived for a deflected beam element as shown in Figure A.

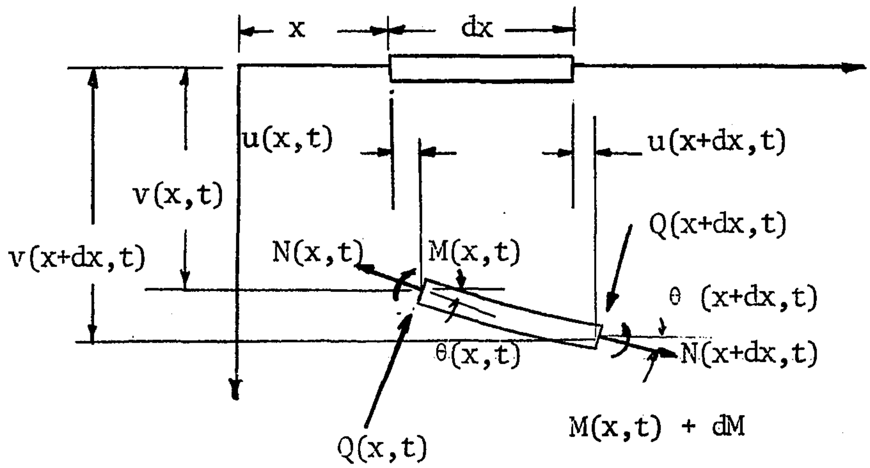

FIGURE A

Summing the forced along the x axis $ma_u = \Sigma F_u$:

$$(\rho A dx)\ \ u,tt = (N + N,_x) \cos\ (\theta + \theta,_x\ dx) - N \cos\theta + Q \sin\theta$$
$$- (Q + Q,_x) \sin\ (\theta + \theta,_x dx) \qquad (1A)$$

Summing the forces along the y axis:

$$(\rho A dx)\ \ v,_{tt} = (Q + Q,_x) \cos\ (\theta + \theta,_x dx) - Q \cos\theta - N \sin\theta$$
$$+ (N + N,_x dx) \sin\ (\theta + \theta,_x dx) + w \qquad (2A)$$

Summing the moments about the element center:

$$J[\theta,_{tt}] = M + dM - M - (Q \cos \theta)[(x + dx) + (u + dx)]$$

$$- (Q \sin \theta)\, dv + (N \cos \theta)dv - (N \sin \theta)\,(dv + dx). \quad (3A)$$

Making the assumption that the change in angle across the element is small enough that the following approximation can be made:

$$\cos (\theta,_{x}dx) = 1$$

$$\sin (\theta,_{x}dx) = \theta,_{x}dx,$$

equation (1A) becomes:

$$(\rho Adx)\, u,_{tt} = (N + N,_{x}dx)\,[\cos \theta - (\theta,_{x}dx) \sin \theta] - N \cos \theta$$

$$+ Q \sin \theta - (Q + Q,_{x}dx)\,[\sin \theta + (\theta,_{x}dx) \cos\theta]$$

$$(\rho Au,_{tt})dx = - (N\, \theta,_{x}dx) \sin\theta + (N,_{x}dx) \cos\theta + (N,_{x}dx)$$

$$(\theta,_{x}dx \sin \theta) - (Q\, \theta,_{x}dx) \cos\theta - (Q,_{x}dx) \sin\theta$$

$$- (Q,_{x}dx)\,(\theta,_{x}dx) \cos \theta. \quad (4A)$$

Neglecting the products of small terms, equation (4A) will reduce to:

$$\rho Au,_{tt} = -(N \sin \theta)\theta,_{x} + N,_{x} \cos \theta - (Q \cos\theta)(\theta,_{x})$$

$$- Q,_{x} \sin \theta,$$

which can be put into the form

$$\rho Au,_{tt} = (N \cos\theta),_{x} - (Q \sin \theta),_{x}. \quad (5A)$$

Apply the same conditions and analyses to equations (2A) and (3A), and the results will be:

$$\rho Av,_{tt} = (N \sin \theta),_{x} + (Q \cos \theta),_{x} \quad (6A)$$

$$J\, \theta,_{tt} = (1 + u,_{x})(Q \cos \theta + N \sin \theta) + v,_{x}\,(N \cos \theta$$

$$- Q \sin \theta) + M,_{x}. \quad (7A)$$

MOMENT-DEFLECTION RELATIONSHIP

The development of the relationship between the moment and deflection, from reference [33], for a simple unrestrained beam includes only the bending strain. For the case when there is stretching and initial load on the beam, the relationship must be modified to include the additional strain.

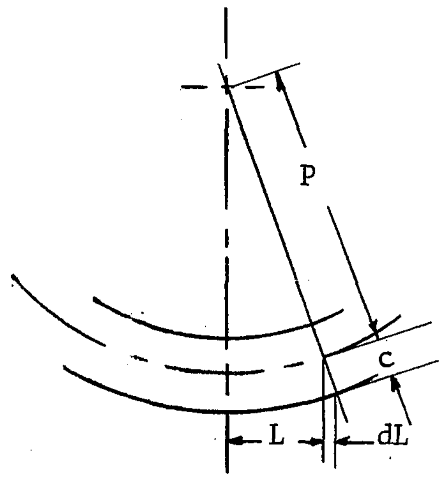

FIGURE B

Figure B indicates a portion of a beam that is deflected in an assumed curved position. The following relationship is derived from the figure:

$$dL/L = c/P. \tag{1B}$$

The term dL/L is defined as the strain on the beam;

$$\text{strain} \equiv dL/L = \varepsilon = c/P,$$

$$1/P = \varepsilon/c. \tag{2B}$$

For an element that has bending and tension strains, the total strains on the outer fibers are:

$$\varepsilon = [N/A + Mc/I]E^{-1}. \tag{3B}$$

STRETCHING LOAD-DEFLECTION RELATIONSHIP

The relationship between the deflection of the beam and the stretching load applied to the beam is derived from the sketch.

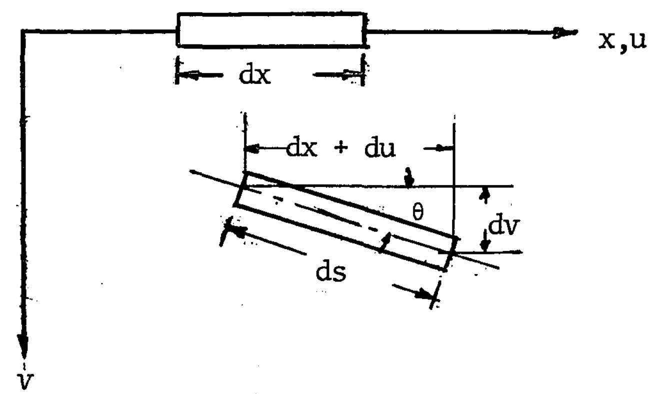

The change in length of the element, dx, is

$$d\ell = ds - dx.$$

The following are determined from the geometry of the figure:

$$ds = [(1 + u,_x)^2 + (v,_x)^2]^{1/2}\, dx,$$

also $$\tan\theta = (v,_x)/(1 + u,_x). \qquad (1C)$$

Boresi [33] presented equation (1C), defining strain in a slightly different manner.

It was assumed and verified by experimental data that the following assumption on the angle was valid:

$$\tan\theta \simeq \sin\theta \simeq \theta \simeq v,_x; \qquad (2C)$$

Comparison of equation (1C) and (2C) indicates that $u,_x$ must be small when compared to unity and can be neglected; therefore,

$$ds = (1 + v,_x^2)^{1/2}\, dx.$$

Expanding the expression and neglecting higher order terms:

$$ds = [1 + (1/2)\ v,_x^2]\ dx,$$

and

$$d\ell = (1/2)\ v,_x^2\ dx.$$

The total elongation of the beam will be

$$\Delta\ell = (1/2)\int_o^\ell v,_x^2\ dx.$$

The strain becomes:

$$\varepsilon_x = \Delta\ell/\ell = (1/2\ell) \int_o^\ell v,_x^2\ dx.$$

The membrane load along the length of the beam is constant (see Figure 23) and can be expressed by:

$$N = (EA/2\ell) \int_o^\ell v,_x^2\ dx, \tag{4C}$$

and the changes in membrane load are

$$N_{,x} = (EA/2\ell)\ v,_x^2 \tag{3C}$$

and

$$N_{,xx} = (EA/\ell)\ v,_x\ v,_{xx}. \tag{5C}$$

EFFECT OF SUPPORT FLEXIBILITY

If the beam is pinned at each end with flexible supports, then the change in length of the system, $\Delta\ell$, becomes:

$$\Delta\ell = \Delta\ell + \Delta\ell_1 + \Delta\ell_2 + \text{---} + \Delta\ell_n,$$

where $\Delta\ell_1$, $\Delta\ell_2$, $\Delta\ell_n$ --- are the displacements of the supports under beam loading. The support system will become effective springs in series with the beam with effective spring constants, k_1, k_2 etc., since the same load is applied to each spring, therefore,

$$\Delta\ell_1 = N/k_1 \quad , \; \Delta\ell_2 = N/k_2 \quad , \text{ etc.}$$

From the analyses on stretching-load deflection relationship

$$\Delta\ell = (n\ell)/EA = (1/2) \int_o^{\ell} v,_x^2 \, dx$$

then
$$\Delta\ell = N\ (\ell/EA) + [(1/k_1) + (1/k_2) + \text{--} + (1/k_n)]$$

$$= (N\ell/EA)\ \{ 1 + (EA/\ell)[(1/k_1) + (1/k_2) + \text{---}$$

$$+ (1/k_n)]\}$$

$$= N\ell/EA'$$

where

$$A' = A/\ \{1 + (EA/\ell)[(1/k_1) + (1/k_2) + \text{---} + (1/k_n)]\}. \qquad (6C)$$

therefore,

$$N = (EA'/2\ell) \int_o^{\ell} v,_x^2 \, dx.$$

If the equation for the effective area, A', is expressed as

$$A' = K_1 A,$$

then the equations for the resonant frequencies will become:

assumed-time mode:

$$\omega^2 = \omega_o^2\ [1 + N_o/P_n + (1.5K_1)R^2]$$

Ritz-Galerkin:

$$\omega^2 = \omega_o^2\ [1 + N_o/P_n + (2.25K_1)R^2]$$

assumed-space mode:

$$\omega = (\pi p)/2K$$

where $p^2 = (n\pi/\ell)^4\ (EI/PA)(1 + 3K_1R^2) + N_o/P_n.$

The function for the stretching stress becomes:

$$\sigma_i = 3K_1R^2P_n/A. \tag{8C}$$

EXPERIMENTAL FLEXIBILITY OF SHAFT AND FIXTURE

Known static loads were applied to the beam and the longitudinal displacement of the shaft supporting the beam ends was measured. These data were used to determine the spring constant of the shaft. The measured spring constant was 30,000 pounds/inch.

The flexibility of the test fixture was measured while subjecting the system to dynamic loads. An accelerometer was located on the pillar block to measure the acceleration in a direction parallel to the beam axis (i.e. motion) and normal to the excitation. The acceleration was measured with and without beam excitation, but both times the fixture was being excited. The difference between the two acceleration measurements was 0.318 g's. The waveform of the acceleration with beam excitation was a sine-squared wave. Integrating the sine-squared wave twice to obtain the amplitude and using the stretching load in the beam, the spring constant of the fixture was 4.3×10^6 pounds/inch. Applying the two spring constants to equation (6C), a value of 0.822 was obtained for K_1.

The modification to the resonant frequencies for the different analytical methods are shown on Figures (16, (17), and (20) and the stretching stress change on Figure (23). The term "modified" means the theoretical analysis modified to account for flexibility of the support (shaft and fixture).

SOLUTION OF BASE EXCITED SYSTEM

Redefining the boundary conditions for a base-excited pin-ended beam as:

$$v\ (x,t) = a_o \sin \omega t \quad \text{at } x = 0, \ell,$$

and

$$v,_{xx}\ (x,t) = 0 \quad \text{at } x = 0, \ell$$

where a_o is the base displacement, the solution of equation (29) becomes (when the assumed-time mode method is used):

$$v\ (x,t) = (a_o + a \sin \alpha x) \sin \omega t. \tag{1D}$$

Substituting equation (1D) into equation (29), the results yield

$$\omega^2 = \omega_o^2\ (1 + 1.5R^2 + N_o/P_n)\ [a \sin \alpha x/(a_o + a \sin \alpha x)]. \tag{2D}$$

APPENDIX B

COMPUTER PROGRAM

Program ran on IBM 360/40

Program Language: Fortran IV

```
C      CALCULATION OF NATURAL FREQUENCIES AND MODE SHAPES
C       OF HINGED BEAMS WITH LARGE AMPLITUDE EXCITATION
       DIMENSION OMEGA(20),STREST(20),OMEGAT(20),OMEGAR(20)
       READ (1,9) T,W,E,XL,XMU
     9 FORMAT(2F10.0,E10.0,F10.0,E10.0)
       WRITE (3,11)
    11 FORMAT(1H1,T18, ' CALCULATION OF NATURAL FREQUENCIES AND MODE SHAP
      1ES'/T19, ' OF HINGED BEAMS WITH LARGE AMPLITUDE EXCITATION')
       WRITE (3,13)
    13 FORMAT (1H0,T11, ' KEY:'//T13, ' OMEGA: RESONANT FREQUENCY FOR SPA
      1CE MODE'/T13, ' OMEGAT: RESONANT FREQUENCY FOR TIME MODE',
      2/T13, ' OMEGAR: RESONANT FREQUENCY FOR RITZ-GALERKIN MODE ',
      3/T13, ' OMEGN: RESONANT FREQUENCY RATIO FOR SPACE MODE ',
      4/T13, ' OMEGNT: RESONANT FREQUENCY RATIO FOR TIME MODE ',
      5/T13, ' OMEGNR: RESONANT FREQUENCY RATIO FOR RITZ-GALERKIN MODE ',
      6/T13, ' STREST: TENSION STRESS CAUSED BY BEAM DEFLECTION ',
      7/T13, ' STRESS: STRESS CAUSED BY DEFLECTION AND INITIAL LOAD ',
      8/T13, ' SO: INITIAL LOAD ',
      9/T13, ' N: MODAL NUMBER ',/T13, ' I: AMPLITUDE RATIO ')
       WRITE (3,12) T,W,E,XL,XMU
    12 FORMAT(1H0,1X,'THICKNESS',T20, ' WIDTH',T35, ' MODULUS',T52, ' LEN
      1GTH',T68, ' MU'//F6.4,' IN.',8X,F5.3,' IN.',4X,  E11.5,' PSI.',3X,
      2F5.0,' IN.',3X,  E10.4)
     1 READ (1,10) SO
    10 FORMAT(F10.0)
       PI = 3.1415927
       XI = W*T*T*T/12.
       B = E*XI
       FCINP = (PI*PI*PI*PI*B)/(XMU*XL*XL*XL*XL)
       SCINP = (PI*PI*SO)/(XMU*XL*XL)
       CINK = (SO*XL*XL)/(PI*PI*B)
       STRC1 = SO/(T*W)
       STRC2 = 3.*(PI*PI*B)/(XL*XL*T*W)
       DO 100 N=1,5,2
       DO 100 IR=1,17
       I = IR-1
```

```
      PS =      (N*N*N*N*FCINP*(1.+3.*I*I)+N*N*SCINP)
      P = SQRT(PS)
      PSS = N*N*N*N*FCINP*(1.+1.5*I*I)+N*N*SCINP
      PSR = N*N*N*N*FCINP*(1.+2.25*I*I)+N*N*SCINP
      IF (I) 31,32,33
   31 STOP
   32 XK = 0
      GO TO 35
   33 XK = SQRT(1./(2.+2.*(1.+CINK/(N*N))/(3.*I*I)))
   35 CONTINUE
      STREST(IR) = STRC2*I*I*N*N
      STRESS = STRC1+STREST(IR)
      CALL CEL1 (CAPK,XK,IER)
      IF (IER) 400,402,401
  400 STOP
  401 WRITE (3,403)
  403 FORMAT (1H0,'K IS NOT IN RANGE -1 TO +1')
      STOP
  402 CONTINUE
      OMEGA(IR) = P/(4.*CAPK)
      OMEGN  = OMEGA(IR)/OMEGA(1)
      OMEGAT(IR) = SQRT(PSS)/(2*PI)
      OMEGNT = OMEGAT(IR)/OMEGAT(1)
      OMEGAR(IR) = SQRT(PSR)/(2*PI)
      OMEGNR = OMEGAR(IR)/OMEGAR(1)
      WRITE(3,200) SO,N,I,OMEGA(IR),OMEGAT(IR),OMEGAR(IR),OMEGN,OMEGNT,
     1OMEGNR,STRESS,STREST(IR)
  200 FORMAT(1H0,T35, ' SO = ',F6.2/T26, ' N = ',I3,T46, ' I = ',I3,
     1//T4, ' OMEGA ',F7.1,' CPS. ',T29, ' OMEGAT = ',F7.1,' CPS. ',
     2T53, ' OMEGAR = ',F7.1,' CPS. '//T4, ' OMEGN = ',F7.1
     3T29, ' OMEGNT = ',F7.1,T53, ' OMEGNR = ',F7.1
     4//T17, ' STRESS = ',E11.5, ' PSI. ',T53, ' STREST = ',
     5E11.5,' PSI. ')
  100 CONTINUE
      GO TO 1
      END
```

```
      SUBROUTINE CEL1(RES,AK,IER)
      IER=0
C     TEST MODULUS
      GEO=1.-AK*AK
      IF(GEO)1,2,3
    1 IER=1
      RETURN
C     SET RESULT VALUE = OFLOW
    2 RES=1.E75
      RETURN
    3 GEO=SQRT(GEO)
      ARI=1.
    4 AARI=ARI
      TEST=AARI*1.E-4
      ARI=GEO+ARI
C     TEST OF ACCURACY
      IF(AARI-GEO-TEST)6,6,5
    5 GEO=SQRT(AARI*GEO)
      ARI=0.5*ARI
      GO TO 4
    6 RES=3.14159265/ARI
      RETURN
      END
```